

pubs.acs.org/Macromolecules Article

Effects of Electrolytes on Thermodynamics and Structure of Oligo(ethylene oxide)/Salt Solutions and Liquid—Liquid Equilibria of a Squalane/Tetraethylene Glycol Dimethyl Ether Blend

Zhengyuan Shen, Qile P. Chen, Shuyi Xie, Timothy P. Lodge,* and J. Ilja Siepmann*



Cite This: Macromolecules 2021, 54, 1120-1136



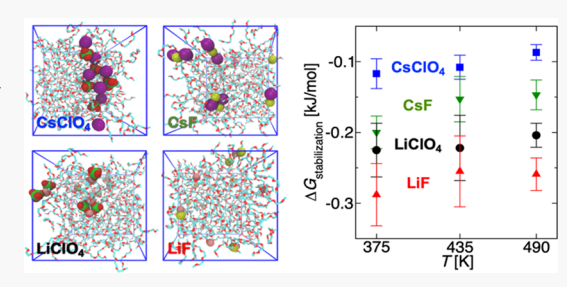
ACCESS

III Metrics & More

Article Recommendations

S Supporting Information

ABSTRACT: Gibbs ensemble Monte Carlo simulations for salt-doped oligo(ethylene oxide) (OEO, $M_{\rm w}=90-266$ g/mol) solutions show that the presence of ions leads to significant increases in the cohesive energy density ($\Pi_{\rm CED}$) and the enthalpy of vaporization for OEO chains but that compensation by entropic contributions leads to only small changes in the Gibbs free energy of transfer and vapor pressure. At the same relative ion concentration (r) and temperature, the $\Pi_{\rm CED}$ values of the salt-doped systems order as ${\rm LiClO_4} > {\rm LiF} > {\rm CsClO_4} \approx {\rm CsF}$. Structural analysis indicates significant ion clustering in addition to coordination of cations by OEO chains. After accounting for ion clustering via the van't Hoff factor, the



solvent vapor pressures are well described by Raoult's law. Experiments and simulations for a squalane/tetraethylene glycol dimethyl ether blend ($x_{W,OEO} = 0.65$) show that the addition of LiClO₄ does not significantly alter the miscibility gap below 0.95 $T_{CP,free}$, the critical temperature of the salt-free blend. However, the coexistence curve for the LiClO₄-doped system does not close with the usual power-law scaling at T > 0.95 $T_{CP,free}$ as transfer of OEO chains to the squalane-rich phase leads to an increase in r in the OEO-rich phase, which, in turn, makes it a less hospitable environment for squalane.

INTRODUCTION

Bicontinuous structures formed by block polymers incorporating blocks with high ion conductivity and with robust mechanical properties are receiving significant attention as potential replacements for conventional liquid electrolytes in rechargeable Li-ion batteries. 1,2 Poly(ethylene oxide) (PEO) is the most commonly used block to achieve high ionic mobility. A detailed understanding of the phase behavior of block polymers with an ion-dissolving block is essential in designing novel battery materials, as well as for optimization of solid-state battery operation.3 However, salt-doped block polymers and homopolymer blends exhibit significant differences in phase behavior from their ion-free counterparts as observed by numerous experimental studies^{4–12} and predicted by theoretical approaches 13-20 and molecular simulations. 21,22 Previous studies revealed that complications arise from preferential solvation of ions^{13,14,20,22,23} along with electrostatic correlations, 15-18 and yet there is still debate regarding the saltinduced segregation and strong asymmetry in the shape of the phase diagram. Theoretical models¹⁴ with emphasis on the aforementioned factors interpret the changes of the phase diagrams of block polymers as a consequence of an increase in the binary Flory-Huggins interaction parameter, χ_{eff} in the presence of salt. Experimental studies¹¹ also invoke nonlinear models of $\chi_{\rm eff}$ as functions of block polymer chain length and salt concentration. However, many issues such as the salt

effects on the microphase-separated morphologies of block copolymers^{24–28} remain to be addressed.

To move toward the goal of predicting order-disorder and order-order transitions and the spatial distribution of ions in block polymer systems, recent studies used salt-doped binary polymer blends as model systems. ^{13,14,19,20,29} The motivation is that the interactions between monomer segments and ions should be representative for both copolymers and blends. Recently, Ren, Nakamura, and Wang¹⁹ developed a numerical mean-field model (called RNW in the following) to predict the impact of salts on polymer blend mixing thermodynamics. The RNW model considers contributions to the free energy of mixing from cation-induced cross-linking, preferential ion solvation, and translational entropy of anions. This model includes several important assumptions: each cation is coordinated by m ether oxygen atoms (where m ranges from 2 to 7), anions are solvated without specific coordination, and ions possess negligible partial molar volume and are not involved in the formation of ion pairs or larger ion clusters. Recently, cloud point and phase coexistence curves have been

Received: October 3, 2020 Revised: November 24, 2020 Published: December 18, 2020





measured experimentally for a series of salt-doped binary polymer blends. ²⁹ Compared to these experiments, the RNW theory provides a good prediction of the coexistence curve of poly(ethylene-alt-propylene)/poly(ethylene oxide) (PEP/PEO) blends doped with lithium bis-(trifluoromethanesulfonyl)imide (LiTFSI) but significantly overestimates the cloud point temperatures at low PEO volume fraction. A consistent overestimation of the miscibility gap is also observed for salt-doped polystyrene/poly(ethylene oxide) (PS/PEO) systems. This suggests the need to improve the theory, as a qualitative description of the phase behavior is not sufficient to enable material design of specific block polymer/salt systems.

One important property for predicting the mixing thermodynamics of two homopolymer components is the Hildebrand solubility parameter (δ) or, equivalently, the cohesive energy density (Π_{CED}). In the Flory–Huggins theory, has separation is enthalpically driven by the difference in δ of each component, and a homogeneous single phase is less favored for systems with larger χ_{eff} . Compared to a salt-free PEP/PEO mixture, the increase in the miscibility gap for PEP/PEO/salt mixtures particularly at high temperatures could be attributed to an increase of the salt concentration in the PEO-rich phase and, as a consequence, a larger χ_{eff} because proportionally more PEO chains than ion pairs transfer to the nonpolar PEP-rich phase.

To obtain microscopic-level insights into macroscopic properties, molecular simulations have been widely utilized to study systems containing alkali metal salts dissolved in PEO.^{34–39} These previous simulation studies have focused on structural and transport properties, particularly cation coordination and diffusion, but have not addressed how the presence of salt affects the thermodynamic properties of the PEO chains.

The purpose of the current simulation study is to obtain a clearer picture of the effect of salts on polymer compatibility, and we examine the influence of salt type and concentration, oligo(ethylene oxide) (OEO) chain length, and temperature on the Π_{CED} of the OEO/electrolyte solutions and on the Gibbs free energy for liquid-to-vapor transfer of the OEO chains. Mixtures of OEO with LiF, LiClO₄, CsF, and CsClO₄ are selected to yield a comprehensive form of Π_{CED} as a function of temperature, chain length, as well as ion concentration. Selection of lithium and cesium cations and fluoride and perchlorate anions allows us to cover small-small, small-large, large-small, and large-large cation-anion combinations. A deeper interpretation of the thermodynamic behavior is achieved through a structural analysis from simulation trajectories that helps to assess the assumptions of the RNW theory. The structural analysis also allows for the determination of van't Hoff factors accounting for ion association that, in turn, allows us to explain trends in the thermodynamics.

METHODS

Calculation of Cohesive Energy Density and OEO Vapor Pressure. Monte Carlo simulations in the canonical (NVT) version of the Gibbs ensemble 40,41 are performed using the in-house Monte Carlo for complex chemical systems—Minnesota (MCCCS—MN) software 42 where only the OEO molecules are allowed to transfer between the two simulation boxes representing the liquid and vapor phases. Simulations are performed on methoxy-group-terminated OEO- $M_{\rm w}$ chains, H-[CH₂-O-CH₂]_n-H, with five molecular weights ($M_{\rm w}=90$, 134, 178, 222, and 266 g/mol, i.e., $2 \le n \le 6$), four different salts (LiF, LiClO₄, CsF, and CsClO₄), at three

temperatures (375, 435, and 490 K), and at one effective salt concentration, defined by the ratio of cations to ethylene oxide (EO) units in only the liquid phase ($r \approx 0.010$, where $r = [\mathrm{M}^+]/[\mathrm{EO}]$, M = Li or Cs). For OEO-222, different salt concentrations are also explored: $r \approx 0.013$ for all four salts, $r \approx 0.019$ and 0.025 for LiClO₄ only, and $r_{\mathrm{tot}} \approx 0.019$ for an equimolar LiF/LiClO₄ salt mixture.

The systems contain either $N_{\rm OEO}^{\rm tot}=188$ OEO molecules for n=2-4 or 200 OEO molecules for n=5 and 6. To achieve an ion concentration close to the desired r value in the liquid phase and a vapor phase containing about 10-20% of the OEO molecules (which allows for the calculation of the saturated vapor pressure with relatively small uncertainties 43), a suitable number of ion pairs is selected first ($N_{\rm salt}\approx r\cdot n\cdot 0.85N_{\rm OEO}^{\rm tot}$). The simulations are initialized with all OEO molecules and ions placed in the liquid phase. Second, the total volume, $V^{\rm tot}$, is adjusted during a pre-equilibration period until r and $N_{\rm OEO}^{\rm ioq}$ fall into the desired range. Numerical values of $N_{\rm OEO}^{\rm tot}$, $N_{\rm salt}$, and $V^{\rm tot}$ and the equilibrium values for $N_{\rm OEO}^{\rm tot}$, $N_{\rm OEO}^{\rm tot}$, $N_{\rm OEO}^{\rm tot}$, and r are provided in Tables S1–S5 in the Supporting Information.

Since we are predominantly interested in understanding the effects of ions of different sizes on OEO chains, relatively simple and computationally efficient models are used in this study. The version of the TraPPE-UA force field modified for ether/alkane mixtures is used to model the OEO chains. 44,45 We use the force fields by Jensen and Jorgensen to model Li⁺, Cs⁺, and F^{-,46} whereas ClO⁻₄ is modeled by the force field developed by Cadena and Maginn. ⁴⁷ Lennard-Jones parameters, partial charges (all ions have a net charge of unity), and bonded interaction parameters are provided in Tables S6 and S7. A spherical cutoff, $r_{\rm cutr}$ at 14 Å is used for the liquid phase of all systems and for the vapor phase when $V^{\rm vap} < 200~{\rm nm}^3$, whereas $r_{\rm cut} \approx 0.4 (V^{\rm vap})^{1/3}$ is used for $V^{\rm vap} > 200~{\rm nm}^3$. For the Lennard-Jones potentials, the interactions beyond the truncation distance are accounted for via analytical tail corrections. ⁴⁸ The Ewald summation method ⁴⁹ with a screening parameter of $\kappa = 3.2/r_{\rm cut}$ and $K_{\rm max} = {\rm int}[\kappa(V_{\rm box})^{1/3}] + 1$ is used to calculate the Coulomb interactions.

Center-of-mass translations, rigid-body rotations around the center of mass for OEO molecules and ClO_4 anions, conformational moves for OEO molecules and anions, volume exchange moves, and particle transfer moves for OEO molecules are used to sample the configurational phase space for the Gibbs ensemble Monte Carlo (GEMC) simulations. The dual cutoff, coupled—decoupled configurational-bias Monte Carlo algorithm 50,51 is utilized to enhance sampling for conformational and particle transfer moves. For the OEO-222 and OEO-266 systems at T=375 K, the acceptance rates for direct phase transfers of these large-chain molecules are prohibitively low. Thus, two each of OEO-90 and OEO-178 molecules are added to improve the sampling via identity switch moves. S2,53 By applying a bias to their transfer free energy, an approximately even distribution of the impurity molecules over the two phases can be achieved. Thermodynamic properties are corrected for the presence of the impurity molecules as described previously.

Eight independent simulations with production periods consisting of at least 1.5×10^5 Monte Carlo cycles (MCCs, where each cycle consists of $N_{\rm OEO}^{\rm tot} + 2N_{\rm salt}$ randomly selected moves) are used to generate all numerical data, and the statistical uncertainties are given as 95% confidence intervals.

The solubility parameter, δ , and cohesive energy density, $\Pi_{\rm CED}$, are defined through the following equations 30,56

$$\delta = \sqrt{\Pi_{\text{CED}}} = \sqrt{\frac{U_{\text{vap}} - U_{\text{liq}}}{V_{\text{liq}}}} = \sqrt{\frac{\Delta H_{\text{vap}} - RT}{V_{\text{liq}}}}$$
(1)

where $U_{\rm liq}$ and $V_{\rm liq}$ are the internal energy and specific volume of the liquid phase, respectively; and $U_{\rm vap}$ and $\Delta H_{\rm vap}$ are the vapor-phase molar internal energy and the enthalpy change upon vaporization, respectively. The third equality applies only at the vapor—liquid coexistence and for systems where the pressure—volume work can be described by the ideal gas law. This is the experimental route to determine δ and $\Pi_{\rm CED}$ values for low-molecular-weight compounds. For polymers, however, the vanishingly small saturated vapor pressure at lower temperatures (below the decomposition temperature) makes

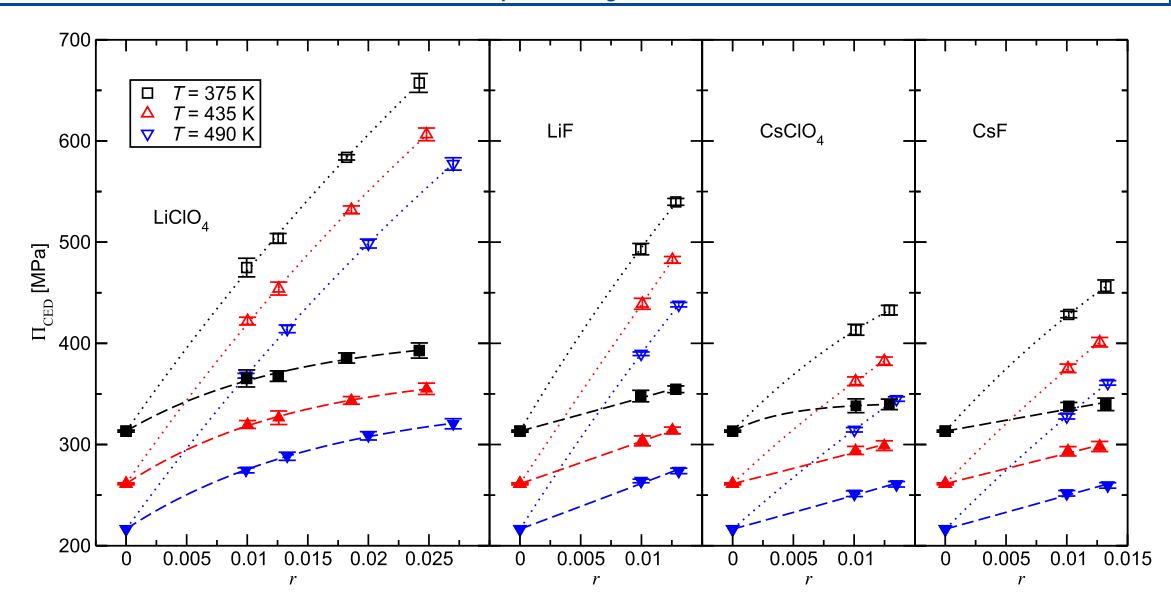


Figure 1. Cohesive energy densities, Π_{CED} , of OEO-222 systems doped with LiClO₄, LiF, CsClO₄, and CsF as a function of ion concentration ($r = [M^+]/[EO]$). Π_{CED} values calculated by the **IP** approach and the corresponding fits (see eq 4) are represented by filled symbols and dashed lines, and those obtained by the **CA** approach are shown as open symbols and dotted lines, respectively. The data for neat OEO-222 (r = 0) are taken from Chen et al.⁴⁴

measurements of $\Delta H_{\rm vap}$ experimentally infeasible, and indirect approaches are used to estimate δ and $\Pi_{\rm CED}$. $^{57-60}$ In contrast, molecular simulation provides an effective approach to accurately calculate δ and $\Pi_{\rm CED}$ via simulations of vapor—liquid phase equilibria or via separate simulations of the liquid phase and of an isolated molecule. 55,59 Previous studies have developed a method to estimate $\Pi_{\rm CED}$ for polymers by extrapolating simulation data for oligomers to obtain infinite-chain-length $\Pi_{\rm CED}$ for polyolefins and PEO. 44,55,61

For the calculation of Π_{CED} for the OEO—salt systems, we use the internal energy form (see eq 1) because neither ΔH_{vap} for the salt nor the excess enthalpy of mixing⁶² is known from the simulations. The liquid-phase properties, U_{liq} and V_{liq} , for the mixture can be taken directly from the GEMC simulations. There are two possible approaches to calculate the internal energy of the vapor phase (with the same composition as the liquid phase) that differ in whether the salt is considered to exist as isolated ion pairs (IP), i.e., a single chemical compound, or as independent isolated cations and anions (CA)

$$U_{\text{vap}}^{\text{IP}} = \langle N_{\text{OEO}}^{\text{liq}} \rangle U_{\text{OEO}}^{\text{iso}} + N_{\text{salt}} U_{\text{ion pair}}^{\text{iso}}$$

$$= (1 - x_{\text{salt}}) \overline{U_{\text{OEO}}^{\text{iso}}} + x_{\text{salt}} \overline{U_{\text{ion pair}}^{\text{iso}}}$$
(2)

$$\begin{split} U_{\text{vap}}^{\text{CA}} &= \langle N_{\text{OEO}}^{\text{liq}} \rangle \ U_{\text{OEO}}^{\text{iso}} + N_{\text{salt}} (U_{\text{cation}}^{\text{iso}} + U_{\text{anion}}^{\text{iso}}) \\ &= (1 - 2x_{\text{cation}}) \overline{U_{\text{OEO}}^{\text{iso}}} + x_{\text{cation}} (\overline{U_{\text{cation}}^{\text{iso}}} + \overline{U_{\text{anion}}^{\text{iso}}}) \end{split} \tag{3}$$

where $N_{\rm salt}=N_{\rm cation}=N_{\rm anion}$ as dictated by neutrality of each phase. For the calculation of $U_{\rm vap}$, $U_{\rm liq}$ and $V_{\rm liq}$, one either consistently uses extensive values or sticks with molar quantities. The IP approach has previously been used to compute the cohesive energy density of ionic liquids because ion pairing in the vapor phase is expected. For the current work, separate Monte Carlo simulations are carried out at each temperature, to obtain the average internal energies for isolated OEO molecules ($2 \le n \le 6$), for each of the four isolated ion pairs, and for an isolated ${\rm ClO}_4^-$ ion; the internal energies of isolated monatomic Li⁺, Cs⁺, and F⁻ ions are zero.

Liquid–Liquid Equilibria (LLE) for Salt-Doped Oligomer Blend. Configurational-bias Monte Carlo simulations 51 in the isobaric—isothermal (NpT) version of the Gibbs ensemble 41 with a three-box setup at p=1 bar are used to simulate the liquid—liquid equilibria (LLE) for an oligomer blend consisting of squalane (representing an (ethylene-*alt*-propylene) oligomer (OEP) with six repeat units) and OEO-222 (containing five repeat units) doped with

LiClO₄. The third box is a vapor phase that facilitates the transfer of oligomers between the two liquid phases. To enhance the sampling efficiency of phase transfers, a series of impurity intermediates of shorter OEP or OEO oligomers are used (see Table S8 for the specific types of intermediate molecules and their numbers). Direct particle transfer moves are only used for the shortest oligomers (i.e., OEP-72 and OEO-90), and the transfer of higher-molecular-weight molecules is achieved via interbox identity switch moves^{52,53} that are applied to all of the neighboring molecular weight oligomer pairs (e.g., OEP-72 and OEP-100). The simulated system consists of 70 squalane molecules, 15 shorter OEP impurity molecules, 274 OEO-222 molecules, 9 shorter OEO impurity molecules, and 14 LiClO₄ units. The total OEO weight fraction is 0.65, and the total ratio of EO units to cations corresponds to r = 0.010. Squalane and the OEP impurity molecules are modeled by the TraPPE-UA force field.⁵¹ The same models as described above are used for OEO molecules and Li and ClO₄ ions.

The simulation is initialized by placing all OEP molecules in the first liquid box and all OEO molecules and the ions in the second liquid box. Center-of-mass translations, center-of-mass rotations, conformational moves, 51 volume moves, and particle transfer and exchange moves between one of the liquid phases and the vaporphase transfer box are used to sample the configurational phase space of the system. The free energies of transfer to and from the vapor phase are biased to ensure that, on average, a sufficient number of each molecule type is present in the vapor phase. Such bias does not affect the resulting liquid-liquid-phase diagram because the same biasing potential is applied to both liquid-vapor box pairs, and its net effect on the liquid-liquid free energy of transfer is thus zero.⁴⁴ It is worthwhile to point out that ions are only present in the OEO-rich phase and are not subjected to transfer moves between boxes. This restriction is motivated by the very small number of ion pairs in the system that would make fractional impurity ions a major perturbation. However, it is important to stress that ion partitioning into the OEOlean phase may not play a major role for a significant part of the phase diagram. Calculations with the RNW model 19 indicate that, for the current system, the r value remains below 0.001 in the OEO-lean phase for $T < 1.1~T_{\rm CP,neat}$ where $T_{\rm CP,neat}$ is the critical temperature of the salt-free oligomer blend. Therefore, on average, less than one ion pair would transfer into the OEO-lean phase for the system size studied here, and the assumption that ions only reside in the OEOrich phase is reasonable.

The LLE simulations are equilibrated for at least 2×10^6 MCCs until there is no drift in energies or compositions for each phase, and the production runs are extended for at least another 5×10^5 MCC. Eight independent simulations were performed, and statistical uncertainties of the simulation data were estimated from these uncorrelated runs and are reported as the 95% confidence interval.

The experimental methods for the determination of the LLE are similar to those used previously by us^{29,44} and are only briefly described here. OEO ($M_n = 222 \text{ g/mol}$) and squalane ($M_n = 423 \text{ g/mol}$ mol) were purchased from the Sigma-Aldrich Corporation. The polymers were dried under dynamic vacuum for 48 h and then stored under static vacuum. $M_{\rm n}$ and MWD of the OEO samples were assessed by matrix-assisted laser desorption/ionization mass spectroscopy (MALDI-MS) and ¹H NMR spectroscopy, and the results are provided in Chen et al. 44 LiClO₄-doped OEO/squalane samples were prepared in 2 mL ampules connected to a Schlenk line. Three quick argon-vacuum cycles were performed to degas the samples, and during the measurement, the samples were protected under argon. Typically, while being vigorously stirred, samples were kept at T = 408K for at least 1 h, followed by slowly cooling to the desired temperature and held there for 1 h. Then, samples were equilibrated for at least 4 h without stirring to attain two coexisting phases and the composition of each phase was analyzed by ¹H NMR spectroscopy.

RESULTS AND DISCUSSION

Cohesive Energy Density. The cohesive energy densities, Π_{CED} , of OEO-222 doped with the four different salts computed using the IP and CA approaches are shown in Figure 1 (numerical values for OEO-222 and other chain lengths are provided in Tables S9-S14). The results from both approaches show that Π_{CED} is a nonlinear and asymptotically increasing function of salt concentration, r. This relationship is especially obvious for the OEO-222/LiClO₄ system, for which the *r* range is extended to higher values. The asymptotic limit is not reached for the salt concentrations investigated here; for LiClO₄, the experimental solubility in PEO is r = 0.16, ⁶⁴ about six times higher than the highest r = 0.027 used in the simulations. Teran and Balsara¹¹ also observed similar behavior for χ_{eff} as a function of r in polystyrene-b-poly(ethylene oxide)/ LiTFSI systems and suggested an inverse exponential dependence. Here, we also find that Π_{CED} for a given chain length (number of heavy atoms, $N_{\rm H}$, or number of EO repeat units, n, where $N_{\rm H} = 3n$) and temperature can be captured by the following equation

$$\Pi_{\text{CED}}(r)|_{N_{\text{H}},T} = \Pi_{\text{CED}}(r=0)|_{N_{\text{H}},T} + \delta_{\text{salt}}[1 - e^{-\epsilon r}]$$
 (4)

where $\delta_{\rm salt}$ and ϵ are adjustable parameters. Our data indicate that a common value of ϵ can be used for all four salts, but that $\delta_{\rm salt}$ needs to be salt-specific.

Comparing the two approaches for calculating U_{vad} , it is obvious that the IP approach yields much smaller Π_{CED} values and $\partial \Pi_{\text{CED}}/\partial r$ slopes than the CA approach because the balance of Coulomb and Lennard-Jones potentials for the ion pair leads to a large shift to lower internal energy than for the isolated cation and anion. Notably, for the OEO-222/LiClO₄ system, a plateau is almost reached at $r \approx 0.025$, and this behavior is in good agreement with the experimental $\chi_{\rm eff}$ behavior. 11 Interestingly, the IP approach also yields much smaller differences between the different salts than the CA approach. This indicates that including ion pairing in the vapor phase may account for part of the differences in the energetics of ion-EO and ion-ion complexation in the liquid phase. Thus, as also done for simulations of ionic liquids, 63 we surmise that the IP approach captures better the energetics of OEO/salt systems, and the remainder of this article focuses on

data obtained from the **IP** approach. For completeness, the results for the **CA** approach are provided in the Supporting Information (see Tables S10–S15 and Figures S1 and S2). For the **IP** approach, Figure 1 points to the following order for the magnitude of the $\delta_{\rm salt}$ coefficients: LiClO₄ > LiF > CsF \approx CsClO₄, and a microscopic-level explanation for this order will be provided later.

The Π_{CED} versus r curves at the three temperatures for a given salt are nearly parallel (see Figure 1), and the r and T dependences can be assumed to be decoupled and, hence, separable. Figure 2 illustrates the temperature dependence of

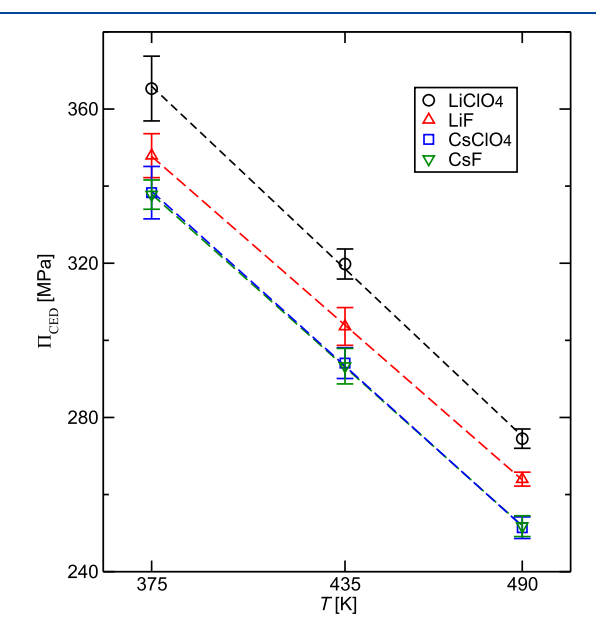


Figure 2. Temperature dependence of $\Pi_{\rm CED}$ for OEO-222 systems doped with LiF, LiClO₄, CsF, and CsClO₄ at an effective ion concentration of $r \approx 0.010$. The dashed lines are linear fits (see eq 6).

 Π_{CED} for the OEO-222/salt mixtures at $r \approx 0.010$. Theoretical studies studies indicate that, for a given chain length and effective salt concentration (including neat oligomers), the Hildebrand solubility parameter, δ , varies linearly with temperature

$$\delta |_{N_{\rm H}, r_i} = \alpha T + \beta \tag{5}$$

This linear dependence for δ leads to a quadratic temperature dependence for Π_{CED} . However, in this case, α is found to be 3 orders of magnitude smaller than β , resulting in a vanishingly small coefficient for the quadratic term. Therefore, a linear correlation is used here also for Π_{CED}

$$\Pi_{\text{CED}}|_{N_{\text{H}},r_i} \approx 2\alpha\beta T + \beta^2$$
 (6)

The $\partial \Pi_{\rm CED}/\partial T$ slopes for the four salts agree within the statistical uncertainties.

Figure 3 illustrates the dependence of Π_{CED} on inverse chain length for OEO/salt systems at three temperatures and $r \approx 0.010$. Previous simulation studies on neat polyolefins have shown a linear relation between Π_{CED} and the reciprocal of the number of heavy atoms (N_{H}) , for $N_{\text{H}} > 10$, $^{5.5,61}$ with a remarkably good agreement between the differences in extrapolated infinite-chain-length Π_{CED} values for different polyolefins and those obtained from small-angle neutron scattering experiments for blends. 55,67 This relationship with respect to inverse molecular weight has been well understood

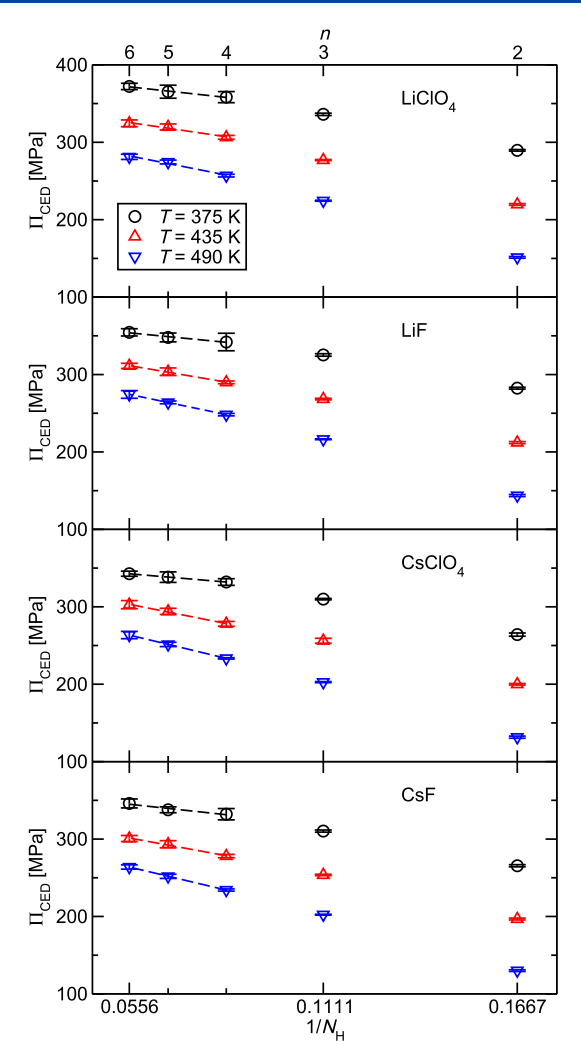


Figure 3. Inverse-chain-length dependence of $\Pi_{\rm CED}$ for OEO systems doped with LiClO₄, LiF, CsClO₄, and CsF at $r\approx 0.010$. The bottom and top x-axes are given as the inverse of the number of heavy atoms, $N_{\rm H}$, and of the number of EO repeat units, n. Dashed lines represent linear fits considering data only for $N_{\rm H} \geq 12$.

by the effect of end group concentration on bulk thermodynamic properties. $^{68-70}$ For the OEO/salt systems, the data for $N_{\rm H}$ = 12, 15, and 18 for each salt at a given temperature are well described by a linear fit. Due to the very small range of inverse $N_{\rm H}$ values, however, the uncertainties in the $\partial \Pi_{\text{CED}}/\partial N_{\text{H}}$ slopes are relatively large. More data extending to $N_{\rm H} \approx 30$ would be needed to allow for a reliable prediction of the infinite-chain-length $\Pi_{\rm CED}$ values. 55 Unfortunately, the simulations for the OEO/salt mixtures are more challenging than those for polyolefins with the same $N_{\rm H}$, and the present fits hold only for relatively low OEO molecular weights. There is a minor temperature dependence in the $\partial \Pi_{\text{CED}}/\partial N_{\text{H}}$ slopes with smaller magnitudes at lower temperatures that has also been observed for oligo-olefins and that is likely related to chain length playing a larger role at higher reduced temperatures $(T/T_{crit})^{.55}$ Given the uncertainties, it appears justified to assume a common $\partial \Pi_{\text{CED}}/\partial N_{\text{H}}$ slope for the four salts at the three temperatures.

The data presented in Figures 1–3 show the dependences of Π_{CED} on r, T, and N_{H} , respectively. To reduce the number of parameters, we assume that these effects can be decoupled over the range of systems (only for $N_{\text{H}} \geq 12$) and state points

investigated here and, hence, Π_{CED} can be modeled by a more comprehensive functional form

$$\Pi_{\text{CED,FIT}}(N_{\text{H}}, T, r)/\text{MPa}$$

$$= A + \frac{B}{N_{\text{H}}} + C(T/\text{K}) + D_{\text{salt}}(1 - e^{-E r})$$
(7)

where Roman letters are used to distinguish coefficients obtained from a comprehensive nonlinear regression to those obtained by individually fitting coefficients for the r, T, and $N_{\rm H}$ dependences, respectively; that is, A accounts primarily for the constant terms from the r, T, and $N_{\rm H}$ dependences but is not the sum of the individual terms. $D_{\rm salt}$ refers to the difference in $\Pi_{\rm CED}$ between the saturated OEO/salt solutions and neat OEO. A fit covering all of the 54 data points with $N_{\rm H} \geq 12$ is shown in Figure 4, and yields mean unsigned and mean

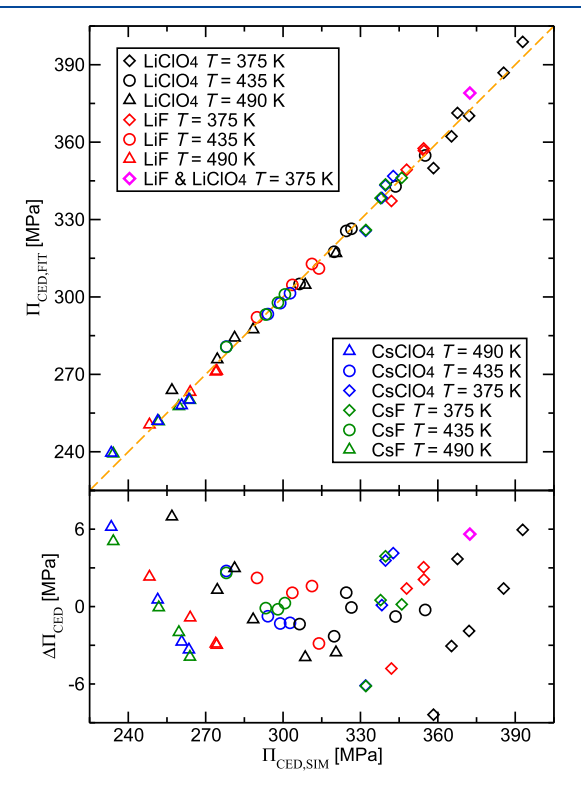


Figure 4. Scatter plot (top) and residuals (bottom) for $\Pi_{\text{CED,FIT}}$ predicted by eq 7 versus Π_{CED} obtained directly from the simulations. Data are shown for $N_{\text{H}} \geq 12$ and distinguished by salt type and temperature but not by chain length and salt concentration.

unsigned percentage errors of 2.8 MPa and 0.8%, respectively. A few data points in the low Π_{CED} regime exhibit slightly greater relative deviations from the fit; these come from shorter chains at higher temperatures. Similar to many other bulk thermodynamic properties, as temperature increases, the domain in which a satisfactory linear fit to reciprocal chain length can be obtained tends to shift to higher molecular weights. The coefficients for eq 7 are listed in Table 1. Since there is some correlation between the individual coefficients, their 95% confidence intervals are estimated by using the 432 data points from 54 systems/state points and 8 independent simulations.

We also performed additional simulations for OEO-222 chains doped with an equimolar LiClO₄ and LiF mixture ($r = r_{\rm LiClO_4} + r_{\rm LiF} = 0.019$) at T = 375 K. Estimating $D_{\rm salt}$ as the

Table 1. Coefficients and Their 95% Confidence Intervals Determined by Fitting to eq 7

A (MPa)	B (MPa)	C (MPa·K ⁻¹)	$D_{\mathrm{LiClO_{4}}}$ (MPa)	$D_{ m LiF}~({ m MPa})$	$D_{\mathrm{CsClO_4}}$ (MPa)	D_{CsF} (MPa)	E
641 ± 5	-740 ± 20	-0.747 ± 0.004	116 ± 3	86 ± 3	60 ± 4	61 ± 4	59 ± 7

arithmetic mean of $D_{\rm LiClO_4}$ and $D_{\rm LiF}$ and using the total ion concentration r, we observed that eq 7 also predicts $\Pi_{\rm CED}$ satisfactorily for this binary salt mixture. This suggests that $\Pi_{\rm CED}$ of systems with more than one type of salt can also be captured reasonably well by this functional form. Thus, eq 7 provides an efficient means to predict $\Pi_{\rm CED}$ values of OEO/salt mixtures containing the four salts investigated here.

The Π_{CED} values of the OEO/salt mixtures, being the enthalpic contribution to $\chi_{\rm eff}$ are a good starting point to understand the effect of salt on the excess free energy of mixing for polymer blends. Decomposing Π_{CED} into contributions from Lennard-Jones and Coulomb potentials indicates that the increase in Π_{CED} upon addition of salt can be mostly attributed to changes in the Coulomb energy, but such a separation needs to be viewed with caution for the effective force fields used here that, for example, may include contributions from orientationally averaged dipole-dipole interactions in the r^{-6} Lennard-Jones term. Furthermore, the Coulomb energy includes contributions from attractive and repulsive ion-ion, ion-EO (where all of the interaction sites carry a partial charge), and EO-EO interactions. The magnitudes of the D_{salt} coefficients for the different salts imply differences in the extent of their influence on Π_{CED} . The trend (LiClO₄ > LiF > CsClO₄ ≈ CsF) could stem from combined effects of both cations and anions. In the RNW model, among the three salt-related contributions to the excess free energy of mixing beyond the usual Flory-Huggins theory, the translational free energy of the anions is assumed to be size-independent, while the Born solvation free energy of the anions is assumed to be inversely related to their size, and the cation contributions are purely entropic. 19 It should be noted that the Born solvation model, while correctly reproducing experimentally observed trends, exhibits a tendency to overestimate the solvation free energy and the immiscibility of liquid mixtures.^{72–74}

Comparing salts with a common cation, the data in Figures 2 and 3 indicate that the Π_{CED} values for OEO/CsF and OEO/CsClO₄ systems are very close and that the OEO/LiF mixture with the smaller anion exhibits smaller Π_{CED} values than OEO/LiClO₄. Comparing salts with a common anion, we observe that doping with Li salts increases Π_{CED} by a larger extent than that with Cs salts. In the next section of this paper, the structural properties of OEO/salt mixtures will be discussed to better understand the role of salts on the cohesive energy density and on polymer blend mixing thermodynamics.

Structural Analysis. Given the smaller size of the cations compared to that of the anions and the more concentrated charge density (or magnitude of the partial charge) on the ether oxygen than on the α -carbon atoms, the cation–EO coordination should play a major role in increasing Π_{CED} upon salt doping. Figure 5 shows the M–O (M = Li⁺ or Cs⁺) radial distribution functions (RDFs) and corresponding number integrals (NIs, the volume integral of the A–B RDF that yields the cumulative number of B atoms/molecules surrounding an A atom/molecule up to distance r) for OEO-222/salt mixtures at $r \approx 0.010$ (see Figure S4 for the X–CH $_x$ RDFs and NIs). The Li–O RDFs show a very pronounced peak at d = 2.1 Å; the height of this peak decreases with temperature but is not strongly affected by the anion type. The first peak in the Cs–O

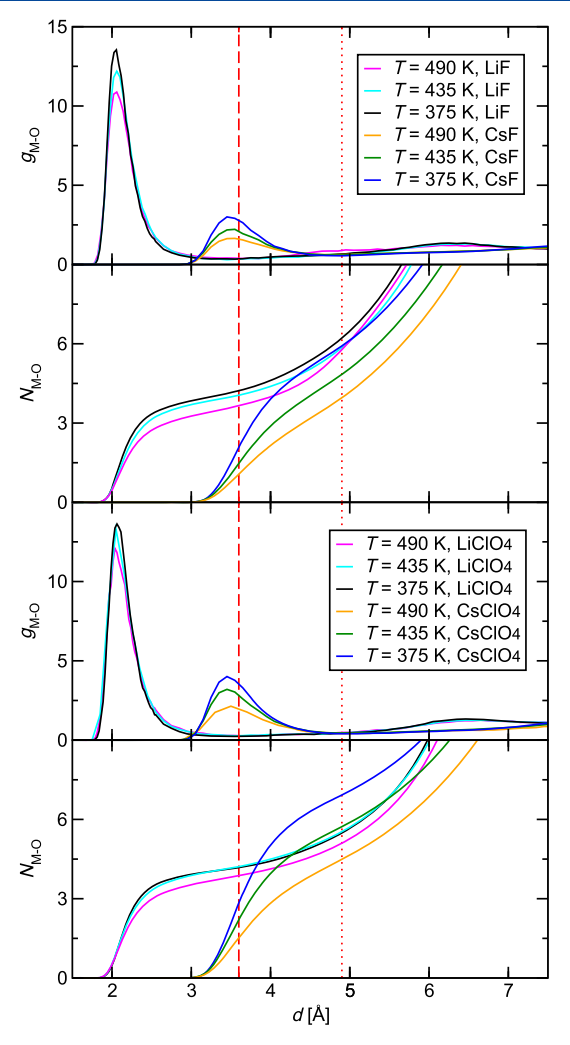


Figure 5. M–O radial distribution functions and number integrals obtained for OEO-222/salt mixtures at $r \approx 0.010$. The dashed and dotted lines represent the Li–O and Cs–O coordination distances, $d_{\rm coord}$ (radius of the first solvation sphere), respectively.

RDFs is much weaker and moved further out to d = 3.5 Å. For the Cs-O RDFs, the relative decrease in peak height with increasing temperature is more pronounced than for the Li-O RDFs, and the peak is significantly higher for CsClO₄ than for CsF.

The coordination number, m, that gives the number of ether oxygen atoms (i.e., excluding the oxygen atoms from ClO_4^-) in the first solvation shell can be obtained from the NI value at the inflection point or at the location of the first minimum of the RDF. The first minimum is more pronounced for the Li–O RDFs, and the coordination distance is found to be $d_{\mathrm{coord}} = 3.6$ Å. The minimum for the Cs–O RDFs is less deep and less well localized; here, a common $d_{\mathrm{coord}} = 4.9$ Å is used for subsequent analysis, but the actual minima for CsClO_4 and CsF are found at 5.0 and 4.8 Å, respectively. Figure 6 shows the temperature dependence of the coordination number for all four salts at $r \approx 0.010$ and for LiClO_4 only also the data at $r \approx 0.025$. There are striking differences between the Li and Cs

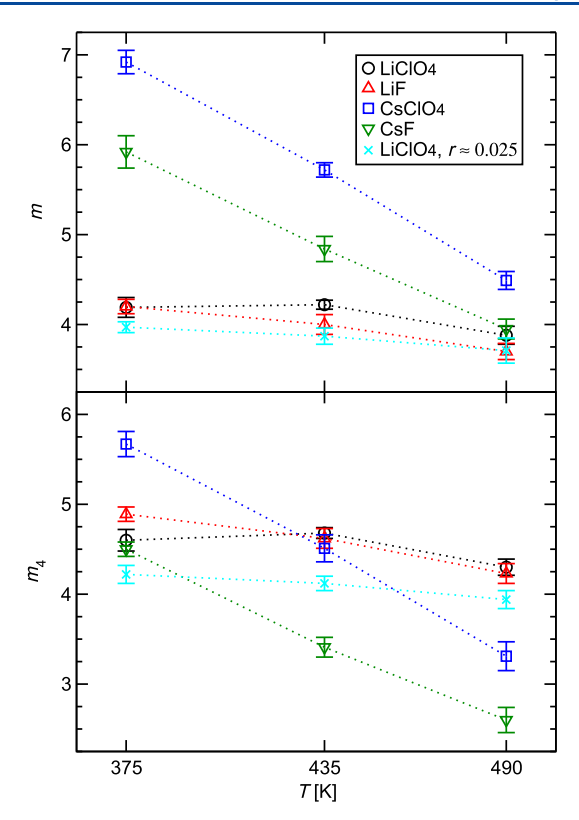


Figure 6. Temperature dependence of (top) m, the M–O coordination numbers, and (bottom) m_4 , the values of the number integral at d=4.0 Å, for OEO-222/salt mixtures at $r\approx 0.010$ and for LiClO₄ only at $r\approx 0.025$.

coordination. The m values for both Li salts at $r \approx 0.010$ are close to 4 and exhibit only a very slight decrease with increasing temperature. In contrast, the m values for the Cs salts at the intermediate temperature are close to 6, decrease by a factor of 1.6 as T is increased from 375 to 490 K, and those for CsF consistently fall below those for CsClO₄.

In the RNW model, the contribution of cation-induced cross-linking to the excess free energy of mixing is assumed to be entirely entropic due to the decreased conformational entropy from M–O complexation with a cation-specific but temperature-independent m value. The simulation data support the assumption of a temperature-independent m value for only the Li salts. Our data indicate a small decrease (\approx 7%) in m for LiClO₄ as r is increased from 0.010 to 0.025 that is consistent with the concentration dependence of the cation coordination observed previously in simulations for PEO/LiClO₄, ^{36,37} PEO/LiI, ³⁴ and PEO/NaI systems. ⁷⁷

Although coordination numbers are usually obtained at the corresponding minimum in the RDF, the difference in $d_{\rm coord}$ (see Figure 5) leads to a volume of the coordination sphere for Cs⁺ that is larger by a factor of 2.5 than for Li⁺. Thus, we also explored the effect of using a common d value for the number integral. Here, we selected d=4.0 Å, the distance beyond which the Cs⁺–O and Li⁺–O interaction energies differ by less than 0.4 kJ/mol \approx 0.1 $k_{\rm B}T$ (see Figure S3). At this common distance, the values of the number integrals are more similar, but the significant temperature and anion effects persist for the Cs⁺ salts (see Figure 6).

The simulations also allow us to assess whether the extent of the M–O coordination depends on the position of the ether group along the chain. Data for OEO-222 with five repeat units

is provided in Table 2. For all four electrolytes, the fractions of M-O coordination involving the O_1 , O_2 , and O_3 ether groups

Table 2. Distribution of M—O Coordination and Fraction of Inter- and Intrachain Cross-Links as a Function of O Atom Location^a for the OEO-222/Salt Systems at T = 435 K and $r \approx 0.01$

	O_1		O_2		O_3	
salt	inter	intra	inter	intra	inter	intra
LiF	0.144	0.242	0.122	0.26_{2}	0.071	0.173
$LiClO_4$	0.161	0.23_{4}	0.16_{3}	0.22_{7}	0.085	0.15_{3}
CsF	0.25_{2}	0.165	0.23_{8}	0.153	0.12_{1}	0.095
CsClO ₄	0.22_{1}	0.17_{1}	0.23_{2}	0.17_{6}	0.11_{3}	0.10_{1}

^aSubscripts give the uncertainty in the last digit as the 95% confidence interval. O_1 , O_2 , and O_3 denote the oxygen atoms for the terminal ether groups, for the ether groups next-nearest to the chain termini, and for the central ether group, respectively, of the EO pentamer.

are close to 0.39, 0.39, and 0.22, respectively, that is, not statistically different from the 2:2:1 ratio of the numbers of these ether groups in a pentamer. Thus, at least, for the oligomers studied here, there does not seem to be a significant positional effect for the M-O location. This negligible positional effect points toward a weak or negligible molecular weight effect for the application of the RNW theory.

The RNW theory 19 disregards the differences between interand intrachain cross-linking. For this analysis, we consider all cross-links made by a given M cation. Taking as example m =5, each of the five oxygen atoms is involved in four cross-links to the other four oxygen atoms, and these four cross-links are then divided into inter- and intrachain fractions. Our simulations indicate that, for the EO pentamer, about 2/3 of the cross-links via Li cations are of the intrachain type, whereas only 2/5 of the cross-links via Cs cations are of the intrachain type. Thus, the larger size of the Cs cations makes intrachain cross-linking more difficult. A significant fraction of interchain cross-linking for Li cations has also been found in recent experimental and simulation studies. 75,76 Comparing between different O atom positions, the simulations yield a slightly larger intrachain cross-link fraction for the O atom at the center of the chain than the two other types of O atoms for all four salts, but these differences mostly fall within the combined uncertainties.

It is intriguing that the Cs^+ salts yield higher coordination numbers but smaller increases in Π_{CED} than the Li^+ salts. This observation indicates that the enthalpic contribution originating from the cation coordination by ether groups is not solely related to the coordination number. If the cation—anion interactions were negligible in the $\mathrm{OEO/salt}$ systems, then the difference in the cation—ether complexation energy could be calculated from the difference in the internal energy of two mixtures sharing the same anion. However, as we will show later, cation—anion interactions are important. In a condensed phase, the M—O binding energy per ion with the coordinating ether oxygen can be computed from the following equation

$$E_{\rm M-O} = \frac{2\pi \rho_{\rm cation}}{N_{\rm cation}} \int_0^{d_{\rm coord}} g_{\rm M-O}(r) u_{\rm M-O}(r) r^2 dr$$
 (8)

where $\rho_{\rm cation}$ is the number density of the cation, and $u_{\rm M-O}(r)$ is the sum of Lennard-Jones and Coulomb interactions. However, $E_{\rm M-O}$ does not include the interactions with the CH_x

groups carrying a partial positive charge. Here, we find $|E_{\rm M-O}|$ values of about 240 kJ/mol for the Li salts and of 72 kJ/mol for Cs salts, i.e., an enormous difference indicating that the Li–O binding is about 3.3 times stronger than the Cs–O binding (see Figure 7). Although there are obvious caveats, we note

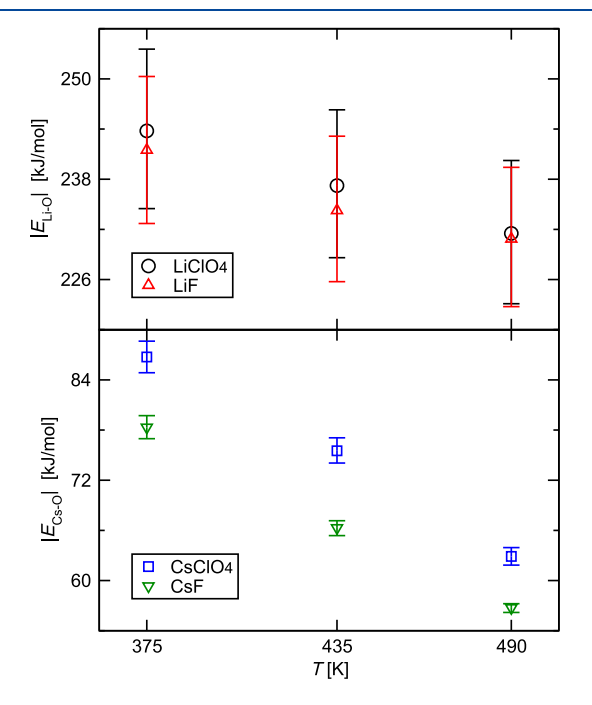


Figure 7. Absolute values of cation—ether oxygen interaction energies for OEO-222/salt mixtures at $r \approx 0.010$.

that our high-temperature, condensed-phase data for $E_{\rm M-O}$ show consistent trends with gas-phase dissociation energies measured by Armentrout and co-workers 78,79 for these cations with two 1,2-dimethoxyethane ligands (384 \pm 21 kJ/mol for Li and 109 ± 8 kJ/mol for Cs, i.e., a ratio of 3.5) and with quantum-mechanical calculation binding energies for optimized clusters (375 kJ/mol for Li and 150 kJ/mol for Cs, i.e., a ratio of 2.5).80 As expected, the $|E_{\rm M-O}|$ values are found to decrease with increasing temperature, where the slope for the Cs salts is about two times larger than for the Li salts. Furthermore, the $|E_{\rm M-O}|$ values are slightly larger for the ${\rm ClO_4}$ salts, i.e., the presence of the smaller fluoride anion reduces the M-O interaction energies. The more favorable E_{M-O} values for the smaller Li cation are likely the main contributor to the larger Π_{CED} for the Li salts (see Figure 2), but there must be secondary factors because the E_{M-O} values for LiF and LiClO₄ are very close, whereas Π_{CED} for LiF is significantly smaller than for LiClO₄.

Changes in the chain conformation are another metric to probe the OEO/cation complexation. For salt-free OEO-222 oligomers, the mean square end-to-end length, $R_{\rm ee}^{-2}$, is approximately 40% of that of the fully extended, all-trans conformation. Addition of LiClO₄ leads to an approximately linear decrease of $R_{\rm ee}^{-2}$ with increasing r (see Figure 8); that is, chelation of a given Li cation by multiple ether oxygens of a given OEO oligomer leads to a contraction of the average chain dimension. Quantum-mechanical studies show globular conformations for a single oligo(ethylene glycol) chain binding to one Li or Cs cation where all five oxygen atoms of the tetramer are found to tightly coordinate the cation. However, at the finite temperature of the simulations and for the r values

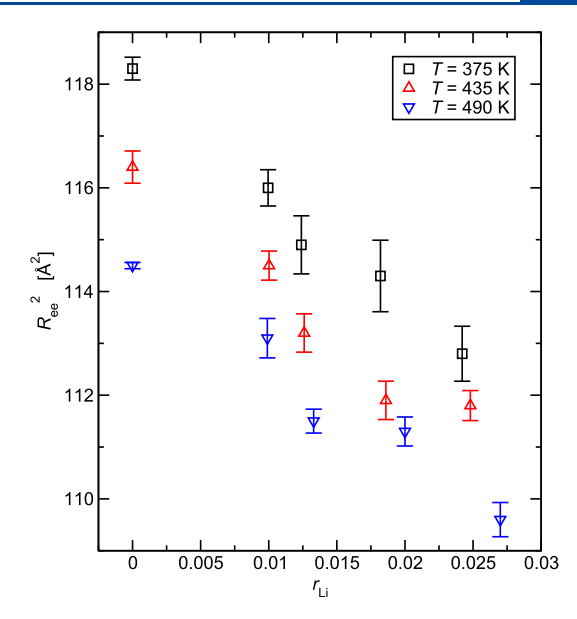


Figure 8. Mean square end-to-end length, $R_{\rm ee}^2$, of OEO-222 oligomers doped with LiClO₄ as a function of ion concentration, $r_{\rm Li}$, at three temperatures.

investigated here, the effect of OEO/cation complexation on chain conformation is relatively minor. Comparing the effects of different salts (see Figure 9), it is evident that the anion type

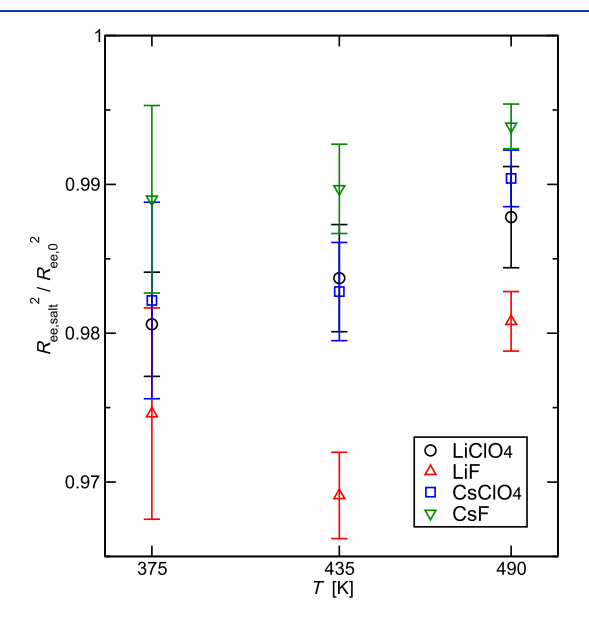


Figure 9. Mean square end-to-end length of OEO-222 chains at $r \approx 0.010~(R_{\rm ee,salt})$ normalized by that of the salt-free system $(R_{\rm ee,0})$ as a function of temperature for different salts.

also plays a role. The relative chain contraction is most pronounced for LiF and least pronounced for CsF with the two perchlorate salts yielding an intermediate contraction. For the latter, there is also no significant difference between Li and Cs cations. As should be expected, a temperature increase leads to a diminishing chain contraction.

Although the difference in the Π_{CED} values between OEO chains doped with Li and Cs salts can be explained as a combined effect of the M–O binding energy (about 3 times larger for Li–O than for Cs–O) and coordination number (about 1.5 times larger for Cs–O than for Li–O), the variation

in the differences between OEO chains doped with F and ClO₄ salts (significant for Li, but negligible for Cs salts) requires further exploration. In particular, M—O coordination numbers are similar for LiClO₄ and LiF salts but different for CsClO₄ and CsF salts (see Figure 6). To further elucidate the differences in the Π_{CED} values, the ion cluster size distributions along with the average cluster sizes are calculated for the four salts dissolved in OEO-222 at $r \approx 0.010$. Here, two ions belong to the same cluster when their separation is smaller than the position of the first minimum in the corresponding RDF (i.e., they form a contact ion pair; see Figure S5) that ranges from 3.0 Å for LiF to 6.5 Å for CsClO₄. As indicated by the data shown in Figure 10 (numerical values are reported in Table

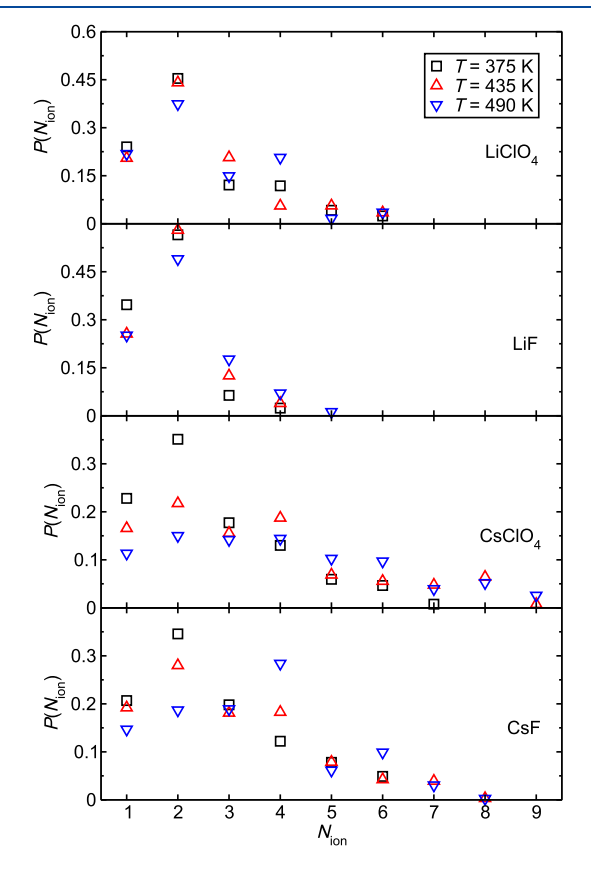


Figure 10. Fraction of ions participating in a cluster consisting of $N_{\rm ion}$ ions in OEO-222/salt mixtures at $r \approx 0.010$. The anion—cation distance cutoffs are 3.0, 4.5, 5.0, and 6.5 Å for LiF, LiClO₄, CsF, and CsClO₄, respectively.

S16), the probability of finding isolated cations or anions ($N_{\rm ion}$ = 1) always falls below 0.35, i.e., more than two-thirds of the ions are part of a cluster. The size distribution also indicates a preference for neutral clusters ($N_{\rm ion}$ = 2, 4, 6, or 8) that is more pronounced at the lowest temperature. The fraction of charged species (free ions or clusters with an odd number of ions) ranges from 0.4 to 0.5 for these systems. Ion clusters were also found by elastic neutron scattering (QENS)⁸¹ and molecular dynamics (MD) simulation studies^{82–84} for PEO-based polyelectrolytes, and in ionic polymer self-consistent field theory (iPSCF), calculations²³ led to estimates of 1.43 and 5.43 nm for the Born solvation radii of positive and negative ions for polystyrene-*b*-poly(ethylene oxide) copolymers doped with LiTFSI that point toward significant ion aggregation.

On average, the fraction of isolated ions decreases and the aggregate size distribution widens as the temperature is increased. These changes result in an increase in the average ion aggregation number with increasing temperature (see Figure 11). Our data show the smallest average ion aggregation

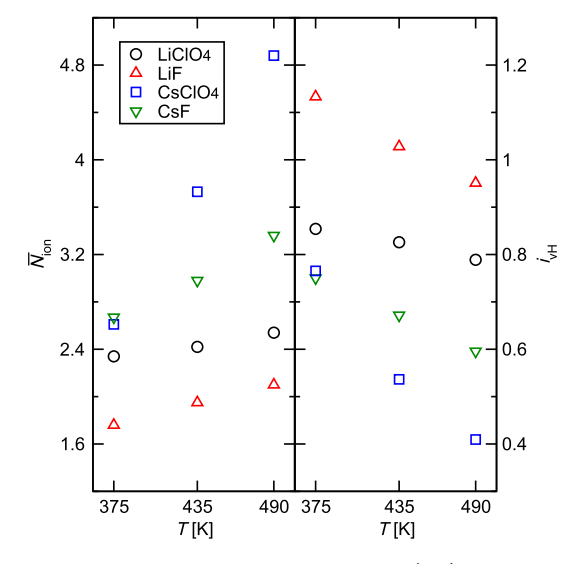


Figure 11. Average ion aggregation number (left) and van't Hoff factor (right) for different electrolytes at $r \approx 0.010$ in OEO-222 as a function of temperature.

numbers for LiF (ranging from 1.8 to 2.1 as the temperature is increased) and the largest aggregation numbers for CsClO₄ (ranging from 2.6 to 4.9). The much larger increase for the Cs salts agrees with the stronger decrease in the M-O coordination numbers, i.e., the weaker binding of the larger cation to OEO leads to more ion-ion aggregation. The simulations for OEO-222/salt mixtures at $r \approx 0.010$ contain a total of 16 cations and anions. Thus, the larger clusters $(N_{ion} \ge$ 7) observed with low frequency for CsClO₄ contain a significant fraction of all ions. Given the preferred ion-ion distance of d = 4.1 Å for CsClO₄ (the first peak position in the corresponding radial distribution function; see Figure S5), a linear cluster with $N_{\rm ion}$ = 10 would be able to span the linear dimension of 4.1 nm for the simulation box. In contrast, even a perfectly linear LiClO₄ with $N_{\rm ion} = 6$ and d = 3.2 Å would still have an end-to-end length less than 2 nm. Most of the ion aggregates assume more globular shapes, and we surmise that the current system sizes are sufficient to capture the ion aggregation.

Comparing OEO-222 systems doped with LiClO₄ at different concentrations (see Figure S6), the extent of aggregation is also strongly influenced by the ion concentration, with the average ion aggregation number increasing from 2.4 at $r\approx 0.010$ to 3.9 at $r\approx 0.025$. An increase in aggregation with increasing temperature is also corroborated by prior MD simulations, ^{34,38,66} as well as IR and Raman spectroscopic studies ^{85–88} on PEO doped with various salts. In addition, these prior studies also found an r dependence on relative populations of free ions and ion pairs/clusters. Experimental cloud point measurements show a slightly larger segregation trend for PEP/PEO doped with LiClO₄ (anion radius 0.240 nm) than with NaI (anion radius 0.206 nm). ²⁹ With smaller anion but larger cation, NaI exhibits weaker ionic behavior by possessing a smaller free-ion fraction than

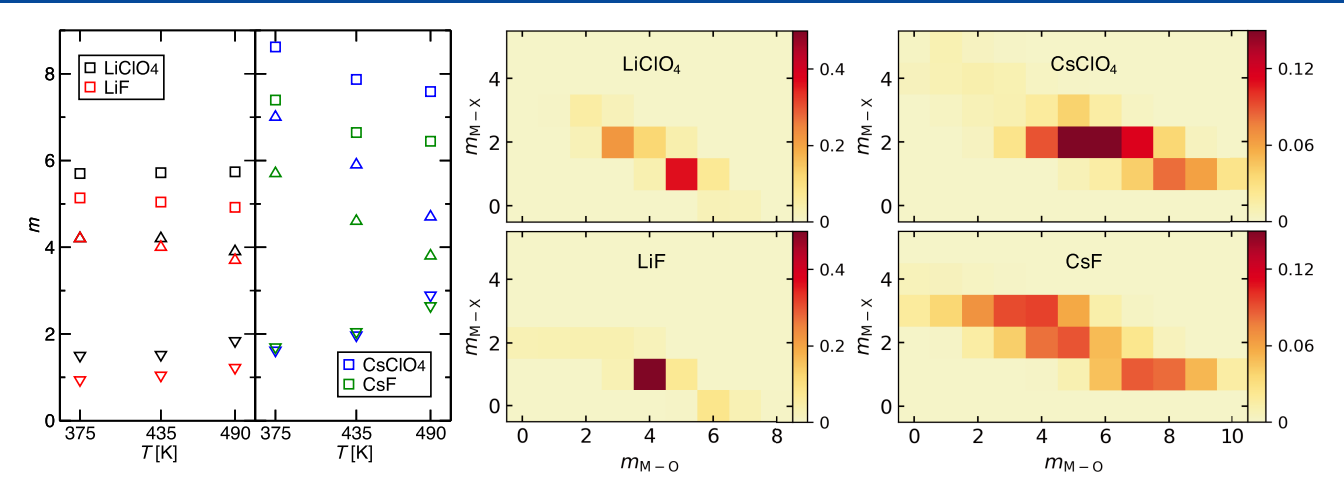


Figure 12. Average coordination numbers (left) for M–O (up triangles), M–X (down triangles), and their sum (squares) as a function of temperature, and two-dimensional (2-D) heat maps for the distributions of M–O and M–X coordination numbers (right) for different electrolytes at $r \approx 0.010$ at T = 435 K. The M–O (M–X) distance cutoffs are 3.6 (3.0), 3.6 (4.5), 4.9 (5.0), and 4.9 (6.5) Å for LiF, LiClO₄, CsF, and CsClO₄, respectively.

LiClO₄. ⁸⁹ This trend is also evident when comparing the present simulation data for LiClO₄ and CsF. In contrast, prior studies for the PEO/LiTFSI mixture containing an even larger anion with significant charge delocalization indicate only a minor extent of ion pairing. ^{3S,90–92} However, the RNW model with its assumptions of no ion pairing and Born solvation free energy leads to an overestimation of the miscibility gap for the PS/PEO/LiTFSI system. ²⁹

Another metric for the extent of ion aggregation is the van't Hoff factor, defined as the ratio of the number (or concentration) of free solute particles in solution over the number (or concentration) of chemical formula units. The van't Hoff factor is a measure of the (nonvolatile) solute's effect on the colligative properties of the solution. For an ideal solution of monovalent ions, as considered here, the van't Hoff factor would be equal to 2. With the exception of LiF, the van't Hoff factors observed here for salts in OEO are less than 1 (see Figure 11), i.e., instead of dissociating into separate cations and anions, the salts aggregate into larger neutral and ionic clusters. Only at the two lower temperatures is net dissociation (a van't Hoff factor larger than 1) observed for LiF. Overall, increasing the bulkiness of the cation or anion leads to a decrease in the van't Hoff factor and a significant population for clusters with $N_{\rm ion} \geq 4$.

Figure 12 shows the M+O coordination numbers and the cation-anion (M⁺-X⁻) coordination numbers, which are computed in the same fashion. For all four salts, the M-O coordination numbers decrease with increasing temperature, whereas the M-X coordination numbers move in the opposite direction. The magnitude of the temperature-induced changes is larger for the Cs salts. Although the M-O and M-X coordination numbers are affected by temperature, the total coordination numbers for the Li salts remain nearly constant. In contrast, the total coordination number for the Cs salts decreases with increasing temperature. In addition to the average coordination numbers, Figure 12 also provides information on the distribution of coordination numbers. The fact that all distributions preferentially align along a diagonal with negative slopes further highlights the competition of anions and ether oxygens to coordinate with cations. For LiF, about 50% of the cations are found to be coordinated at the same time to one anion and four ether oxygens. The

distributions are much more spread out for the Cs salts. For CsF, M-O+M-X counts of 7+1, 5+2, and 4+3 are nearly equally prevalent. Again, it needs to be emphasized that there is no unique criterion for comparing coordination across different species; here, we use distance cutoffs based on the first minimum in the corresponding RDF.

Based on our structural/energetic analysis, the small differences in $\Pi_{\rm CED}$ of OEO mixtures determined with the IP approach for different salts can be qualitatively explained through an interplay of two factors. First, the smaller Li cation allows for the formation of a tighter and energetically much more favorable coordination to the ether oxygens (see Figures 5 and 7), and this leads to larger $\Pi_{\rm CED}$ values. Second, comparing the two Li salts, there is more ion—ion aggregation for LiClO₄, and this leads to its higher $\Pi_{\rm CED}$ values compared to LiF.

Transfer Thermodynamics. The two-box GEMC simulations also allow for a direct assessment of the effects of salt on the excess chemical potential and vapor-to-liquid transfer properties for OEO chains. Given the extremely low vapor pressure of the OEO chains, the vapor phase can be assumed to be an ideal gas and, hence, the Gibbs free energy of transfer, $\Delta G_{\rm trans}$, is a direct measure of the excess chemical potential. Here, $\Delta G_{\rm trans,OEO}$ for OEO molecules is calculated directly from the partition coefficient $^{93-95}$

$$\begin{split} \Delta G_{\text{trans,OEO}} &= \Delta G_{\text{vap} \rightarrow \text{liq,OEO}} = \mu_{\text{OEO}}^{*,\text{liq}} - \mu_{\text{OEO}}^{*,\text{vap}} \\ &= -k_{\text{B}} T \ln \left(\frac{\langle \rho_{\text{liq,OEO}} \rangle}{\langle \rho_{\text{vap,OEO}} \rangle} \right) \end{split} \tag{9}$$

where $\mu_{\text{OEO}}^{*,\text{liq}}$ and $\mu_{\text{OEO}}^{*,\text{vap}}$ are the so-called pseudo-chemical potentials 3,94 for OEO molecules in the liquid and vapor phases, respectively; k_{B} is the Boltzmann constant; and $\langle \rho_{\text{liq,OEO}} \rangle$ and $\langle \rho_{\text{vap,OEO}} \rangle$ are the ensemble-averaged number densities of OEO molecules in the liquid and vapor phases, respectively, from the GEMC simulation. The should be noted that $\rho_{\text{liq,OEO}}$ and $\rho_{\text{vap,OEO}}$ are mechanical properties that are available for every step of the GEMC trajectory and that the transfer free energy computed from eq 9 is much less affected by finite-size effects than the chemical potential obtained via ghost particle insertions. Equation 9 does not invoke a standard state and can be applied to transfer processes at any

mole fraction of the species of interest including a unary system. 93,94 It is important to have a quantitative metric that applies at any arbitrary concentration. For example, when the OEO molecules are divided into one tagged molecule and N-1 untagged molecules, then the vapor pressure of this solution must be exactly the same as that for a unary system, and the partition coefficients of the tagged and untagged molecules must be equal.

With knowledge of the large effect of electrolytes on Π_{CED} , the expectation is to also find large shifts for $\Delta G_{\text{trans,OEO}}$. However, as shown in Figure 13, only very small differences

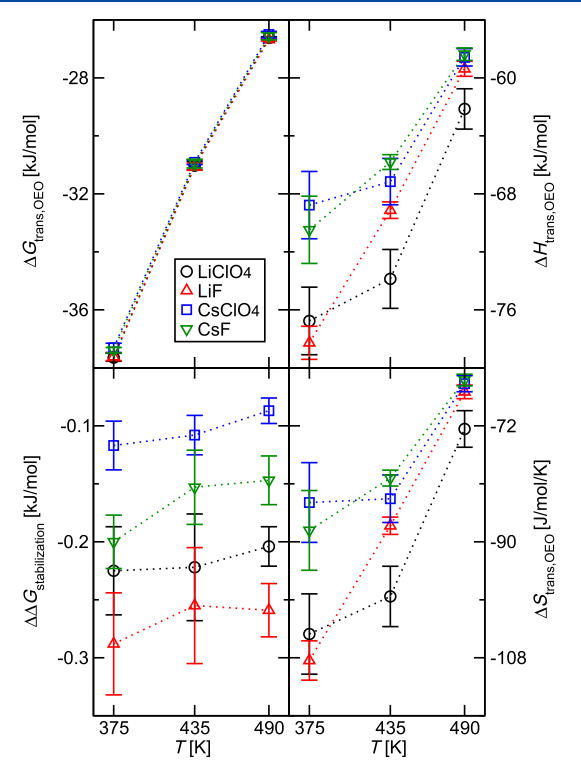


Figure 13. Thermodynamic vapor-to-liquid transfer properties for OEO-222 molecules obtained for different electrolyte solutions at $r \approx 0.010$ as a function of temperature: (top left) Gibbs free energy of transfer, $\Delta G_{\rm trans,OEO}$; (top right) enthalpy of transfer, $\Delta H_{\rm trans,OEO}$; (bottom right) entropy of transfer, $\Delta S_{\rm trans,OEO}$; and (bottom left) stabilization Gibbs free energy, $\Delta G_{\rm stab,OEO}$. The dashed lines are used to guide the eye.

between $\Delta G_{\rm trans,OEO}$ for different electrolytes are observed for the OEO-222/salt mixtures. The enthalpy of transfer, $\Delta H_{\rm trans,OEO}$, can be determined as follows

$$\Delta H_{\text{trans,OEO}} = H_{\text{OEO}}^{\text{liq}} - H_{\text{OEO}}^{\text{vap}}$$

$$= \frac{\partial H^{\text{liq}}}{\partial N_{\text{OEO}}} |_{N_{\text{ion}}, N_{\text{imp}}} - \frac{\partial H^{\text{vap}}}{\partial N_{\text{OEO}}} |_{N_{\text{ion}}, N_{\text{imp}}}$$
(10)

where $H_{\mathrm{OEO}}^{\mathrm{liq}}$ and $H_{\mathrm{OEO}}^{\mathrm{vap}}$ are the partial molar enthalpies of an OEO molecule of interest in the liquid and vapor phases, respectively. The partial molar enthalpy is obtained by taking the partial derivative of the average system enthalpy in a given simulation box for a specific number of ions and impurity molecules with regard to the number of OEO molecules. Since ions are not allowed to transfer between the two simulation boxes, only N_{OEO} and N_{imp} fluctuate throughout a simulation trajectory. Note that $H_{\mathrm{OEO}}^{\mathrm{liq}}$ does not include a contribution

from direct ion—ion interactions, whereas $U_{\rm liq}$ entering into the calculation of $\Pi_{\rm CED}$ includes all interactions (see eqs 1 and 2). Once $\Delta G_{\rm trans,OEO}$ and $\Delta H_{\rm trans,OEO}$ are known, the entropy of transfer is calculated from

$$\Delta S_{\text{trans,OEO}} = \frac{\Delta H_{\text{trans,OEO}} - \Delta G_{\text{trans,OEO}}}{T}$$
(11)

Despite the relatively large uncertainties, the $\Delta H_{\rm trans}$ values (see Figure 13) suggest that the liquid phases containing Li salts provide an enthalpically more favorable environment for OEO chains than those with Cs salts. In addition, the order of $|\Delta H_{\rm trans,OEO}|$ (LiClO₄ > LiF > CsF \approx CsClO₄) also agrees with the trend in $\Pi_{\rm CED}$ values. Indeed, as shown in Figure S7, there is a remarkable correlation between $|\Delta H_{\rm trans,OEO}|$ and $\Pi_{\rm CED}$ values for the data at T=435 and 490 K but some deviations from linearity for the larger salts at 375 K. This correlation holds only for the $\Pi_{\rm CED}$ values obtained with the IP approach. The pronounced temperature dependence of the $\Delta H_{\rm trans,OEO}$ values calculated from the calorimetric formula (eq 10) signals that great caution would be needed when attempting to obtain $\Delta H_{\rm trans,OEO}$ via the van't Hoff relation from the temperature dependence of the partition coefficient.

Since $\Delta G_{\rm trans,OEO}$ values are similar, but $\Delta H_{\rm trans,OEO}$ values differ among the electrolytes, there must be enthalpy—entropy compensation and the behavior for $\Delta S_{\rm trans,OEO}$ closely matches that for $\Delta H_{\rm trans,OEO}$ (see Figure 13). Clearly, the vapor-to-liquid transfer into a solution containing Li ions is enthalpically favored compared to that with Cs ions, but the strong Li–O interaction also results in an increased entropic penalty. As temperature increases, there is less cation coordination by the OEO chains, and the entropic penalty becomes smaller. The large degree of enthalpy—entropy compensation is consistent with the experimental observation that the shape of the phase diagram for binary PEP/PEO is not very sensitive to the type of the doped salt at the same salt concentration. ²⁹

Although the differences in $\Delta G_{\rm trans,OEO}$ for different electrolytes at the same r are rather small, they are still statistically significant. To highlight the effect of the electrolytes, it is instructive to compare $\Delta G_{\rm trans,OEO}$ values for solvation in neat and salt-doped OEO systems, and we define a stabilization free energy as follows

$$\Delta \Delta G_{\text{stab,OEO}} = \Delta G_{\text{trans,OEO}}^{\text{salt}} - \Delta G_{\text{trans,OEO}}^{\text{salt-free}}$$
 (12)

As shown in Figure 13, $\Delta\Delta G_{\text{stab,OEO}}$ is negative for all four salts, i.e., solvation in the salt-doped mixtures is more favorable than self-solvation of OEO chains. The $\Delta\Delta G_{ ext{stab,OEO}}$ values are most negative for LiF and least negative for CsClO₄. Smaller cations and anions lead to a more favorable solution environment, and the effect of cation size is more pronounced than that for anions (a 0.11 kJ/mol difference between LiX and CsX pairs versus a 0.06 kJ/mol difference between MF and MClO₄ pairs). It should be noted that the $\Delta\Delta G_{\text{stab,OEO}}$ values are obtained here for relatively short oligomers. For a fixed r(salt concentration per EO segment), the number of cations coordinated to a given OEO chain should increase with increasing chain length. Data for the LiClO₄-doped system (see Figure S8) indicate that $\Delta\Delta G_{\text{stab,OEO}}$ values decrease linearly for $n \ge 3$. Thus, a significant salt-induced stabilization should be expected for higher-molecular-weight EO polymers.

Figure 14 shows the reduced vapor pressures of OEO-222 chains doped with the four salts, over the vapor pressure of neat OEO-222, as a function of the effective mole fraction.

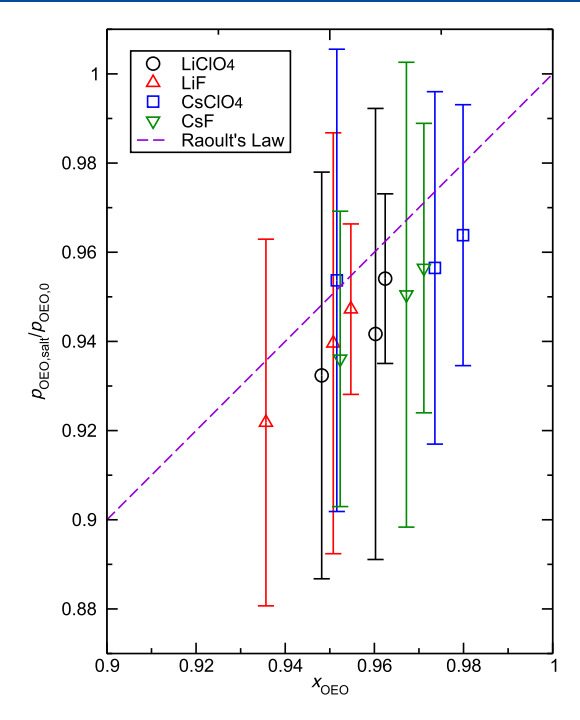


Figure 14. Reduced vapor pressure of OEO-222 chains for different electrolyte solutions at different temperatures and $r \approx 0.010$ shown as a function of its effective mole fraction accounting for the presence of ion aggregates. The purple dashed line represents Raoult's law.

This calculation accounts for the numbers of cations and anions as prescribed by the van't Hoff factor and, only at $T=375~\rm K$, also for the presence of small numbers of OEO-90 and OEO-178 impurity molecules. Although the relative uncertainties are quite large, the reduced vapor pressure is well described by Raoult's law. This result strongly supports that using the locations of the first minimum in the cation—anion radial distribution functions as ion-pair-specific distance cutoffs yields a thermodynamically consistent approach to determine ion aggregates, whereas using a common cutoff distance for

different ion pairs would yield thermodynamically inconsistent results. Evidently, the differences in $\Delta\Delta G_{\rm stab,OEO}$ between different ions at the same r are mostly a consequence of the differences in ion aggregation, and they are greatly diminished when comparing different electrolytes at the same concentration of ion aggregates (i.e., using $r \times i$ instead of r).

Liquid-Liquid Equilibria. Figure 15 depicts the coexistence curves for salt-free and LiClO₄-doped squalane/OEO-222 mixtures ($x_{\text{W.OEO}} = 0.65$ and $r_{\text{total}} = 0.010$) obtained from experiments, molecular simulations, and predictions of the RNW theory (numerical data for experiments and simulations are provided in Tables S17 and S18). A reduced temperature scale is used to provide better visual comparison by accounting for the overestimation of the critical temperature of the neat system from simulations using nonpolarizable force fields $(T_{\text{CP,neat}} = 355 \text{ and } 430 \text{ K for experiment}^{29} \text{ and simulation}^{44}).$ For the RNW theory, 19 the following model parameters are used: $\chi_{\text{eff}} = 540 \text{ K/}T - 1.15$ (with a reference volume of 100 Å³);²⁹ an anion radius of $R_{\text{anion}} = 0.24 \text{ nm}$;^{97,98} and two values for the Li–EO coordination number, m = 2 and 5.²⁹ It is very encouraging that experiment, molecular simulation, and RNW theory yield very consistent shapes for the LLE data of the saltdoped oligomer blend. The remarkable agreement with the RNW theory developed for polymer blends may be due to the negligible positional effect on the M-O coordination observed for the oligomers (see Table 2).

The coexistence compositions are only slightly shifted from those of the salt-free blend at $T\approx 0.95~T_{\rm CP,neat}$. The slight outward shift is more apparent for the OEO-rich phase; that is, the solubility of squalane in the OEO-rich phase is more affected than the solubility of OEO-222 in the squalane-rich phase by the presence of LiClO4. The latter is in agreement with the small $\Delta\Delta G_{\rm trans,OEO}$ for OEO observed for the vapor—liquid equilibria. However, at $T\approx 0.95~T_{\rm CP,neat}$, the shape of the coexistence curve for the LiClO4-doped mixture starts to diverge from that of the salt-free system. For the LiClO4-doped mixture, there is an inflection point in the coexistence curves at $T\approx 1.02~T_{\rm CP,neat}$ and above that, the miscibility gap depends

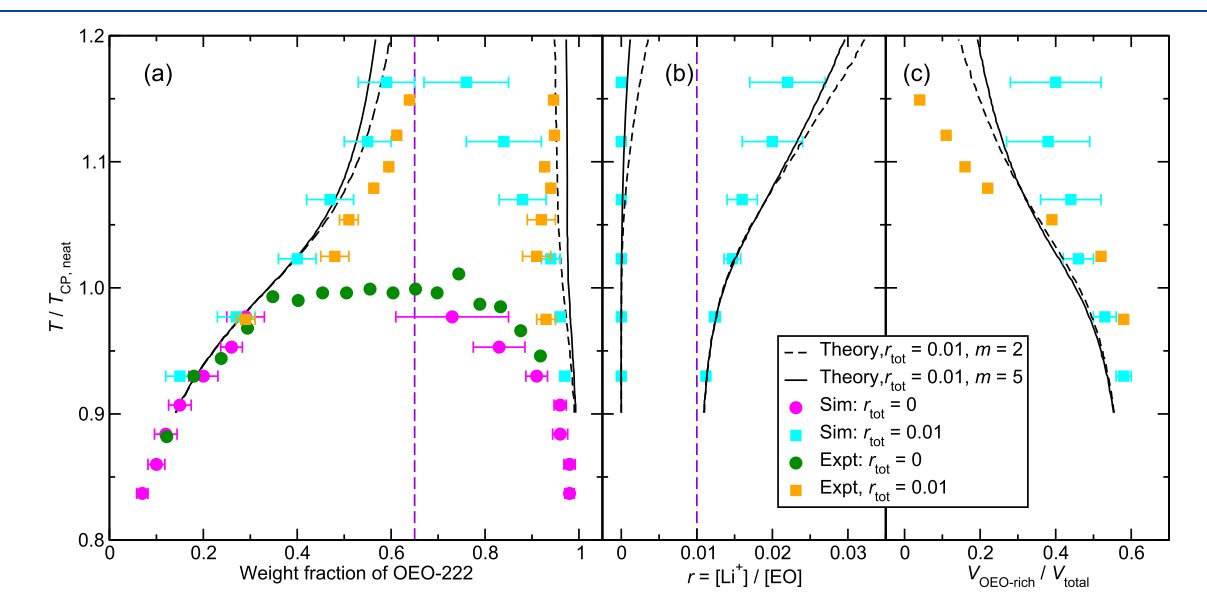


Figure 15. Coexistence curve (a), ion concentration (b), and volume ratio (c) for the squalane/OEO-222 mixture doped with LiClO₄. The dashed lines indicate the overall OEO-222 and ion concentrations. The experimental and simulation data for the salt-free mixture are taken from refs 29 and 44.

only weakly on temperature. A similar change in the shape of the coexistence curve was previously observed for PEP/PEO/ LiTFSI mixtures. 29

The RNW theory yields a slightly wider miscibility gap than experiment and simulation. Although not very sensitive to the choice of coordination number, the predictions using m = 2 are in slightly better agreement with the experimental data. Here, it should be noted that the simulations indicate about two interchain cross-links when $r \approx 0.01$. Below the inflection point, the simulations underestimate $x_{W,OEO}$ in the squalanerich phase and overestimate it in the OEO-rich phase. However, at higher $T/T_{\rm CP,neat}$, the simulations exhibit a more pronounced decrease in $x_{W,OEO}$ for the OEO-rich phase. The temperature dependence of the relative ion concentration, r, is also shown in Figure 15. Since ion transfers are not attempted, r in the squalane-rich phase is always zero for the simulations, but the differences with the theory prediction are fairly small below $T \approx 1.1 T_{\text{CP.neat}}$. More importantly, the simulation and theory curves for r(T) in the OEO-rich phase trace each other closely and show a monotonic increase with increasing T. This increase in ion concentration is caused by the Gibbs free energy of transfer from OEO-rich to squalane-rich phase being much more unfavorable for LiClO₄ than for OEO. As $x_{W.OEO}$ in the squalane-rich phase approaches the overall value of 0.65, the volume fraction of this phase increases (see Figure 15). The concurrent decrease in $V_{\mathrm{OEO-rich}}/V_{\mathrm{total}}$ is more pronounced for the experimental data than for theory and simulation above $T \approx 1.03~T_{\rm CP,neat}$. As dictated by the lever rule, the decrease of $V_{\mathrm{OEO-rich}}/V_{\mathrm{total}}$ is less severe for the simulations at high temperatures.

The Gibbs free energies of transfer for squalane and OEO-222 molecules can be calculated directly from the corresponding number densities (see eq 9). In particular, the three-box GEMC simulations allow us to decompose the liquid-to-liquid transfer free energies into separate liquid-to-vapor (desolvation) and vapor-to-liquid (solvation) terms. The data in Figure 16 are presented in such a manner that the transfer direction leads to negative values for ΔG_{trans} . In general, ΔG_{trans} values for squalane are larger in magnitude than the corresponding values for OEO-222 molecules; this even holds for the vaporto-OEO-rich-liquid transfer. The reason is likely the difference in chain lengths; squalane consists of six EP repeat units, whereas OEO-222 consists of only five EO units, and each of the EP units includes five heavy atoms (versus three for the EO units). Below $T_{\rm CP,neat}$ (≈ 430 K), the $\Delta G_{\rm vap \to SQ}$ values for both OEO-222 and squalane are not significantly affected by the addition of salt, which is expected because there are no ions in either phase and $x_{W,OEO}$ is only slightly smaller in the squalanerich phase for the LiClO₄-doped system. For the vapor-to-OEO-rich phase transfer, the $\Delta G_{\text{vap}\rightarrow EO}$ values for OEO-222 are slightly shifted down for the salt-doped system compared to those for the salt-free system. The most significant change is that, as $T_{\text{CP,neat}}$ is approached from below, the $\Delta G_{\text{vap}\to \text{EO}}$ values for squalane in the salt-free system decrease concurrently with the rapid increase in $x_{W,SQ}$, whereas the $\Delta G_{\text{vap}\to EO}$ values for squalane continue to increase for the LiClO₄-doped system. Since the salt-doped OEO phase is a less favorable solvation medium for squalane, its concentration remains low in the OEO-rich phase even as the temperature increases. As a consequence, the effect of salt on $\Delta G_{\text{liq} \rightarrow \text{liq}}$ is significantly more pronounced for squalane than for OEO-222. That is, the significant increase in Π_{CED} values for the OEO phase upon addition of salt makes it less compatible for the uptake of

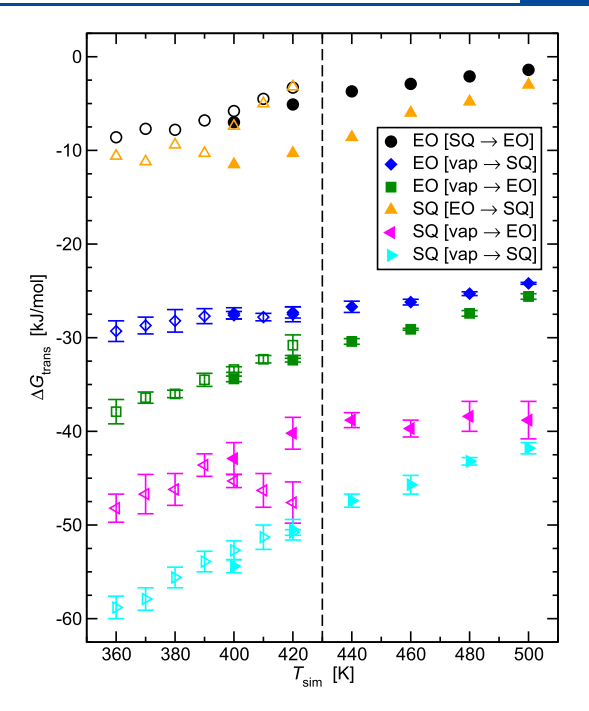


Figure 16. Gibbs free energies of transfer for OEO-222 and squalane molecules as a function of temperature. Data are shown for liquid-to-liquid, vapor-to-squalane-rich, and vapor-to-OEO-rich transfers. Open and filled symbols represent data for salt-free and LiClO₄-doped mixtures, respectively. The dashed line indicates $T_{\rm CP,neat}$ -

squalane, whereas enthalpy—entropy compensation partially mutes its effect on the escaping tendency of OEO. As temperature increases, more OEO molecules migrate into the squalane-rich phase than squalane molecules transfer into the OEO-rich phase. Thus, the coexistence curve is shifted to the side with higher $x_{W,OEO}$. Based on linear extrapolation, the $\Delta G_{\text{liq} \rightarrow \text{liq}}$ values would reach zero at $T \approx 530$ K and the miscibility gap should close.

Since the relative ion concentration increases with increasing temperature for the LLE setup (see Figure 15) and since OEO coordination to Li cations becomes less strong with increasing temperature (see Figure 12), we expect ion aggregation to rapidly increase in the OEO-rich phase. Indeed, the data shown in Figure 17 demonstrate pronounced changes in the aggregate size distribution as the temperature is increased. At $T/T_{\rm CP,neat}$ = 0.93, about one-third of the ions are not in direct contact with an oppositely charged ion, about half of the ions are found as neutral ion pairs, and about one-eighth are found as charged trimers. At $T/T_{\rm CP,neat}$ = 1.02, the fraction of unassociated ions is only about 10% and neutral 4-, 6-, and 8mers become important, whereas the fractions of dimers and trimers are similar to the lower temperature. At $T/T_{\rm CP,neat}$ = 1.12, aggregation as tetramer becomes most prevalent, followed by dimers and hexamers, and less than 3% of the ions are unassociated or part of a charged trimer. These results are consistent with infrared and Raman spectroscopies^{85,86} and simulations³⁶ for the PEO/LiClO₄ mixture. Concomitant with the increase in ion aggregation, the LLE simulations also show a decrease in the Li–EO coordination number from 5.4 at T/ $T_{\rm CP,neat} = 0.93$ to 2.8 at $T/T_{\rm CP,neat} = 1.12$. Although the predictions of the RNW model are very satisfactory (see Figure 15), the formation of ion aggregates and the variation in the degree of Li-EO cross-linking stand in contrast to the assumption underlying the RNW model.

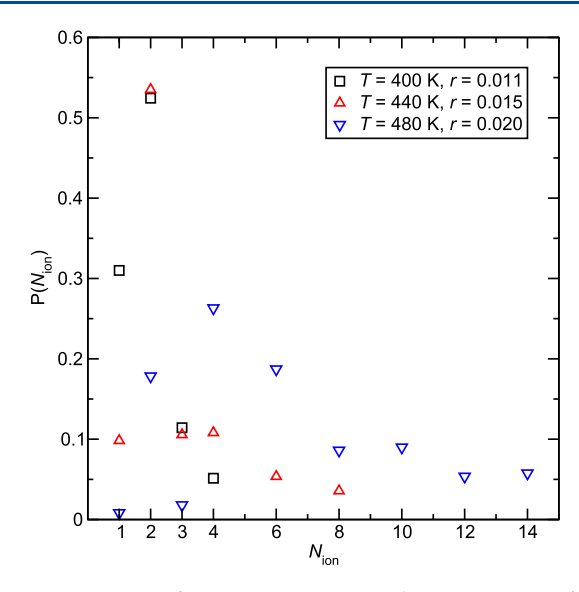


Figure 17. Fraction of ions participating in a cluster consisting of $N_{\rm ion}$ ions in the OEO-rich phase for the squalane/OEO-222/LiClO₄ system at T=400, 440, and 480 K ($T/T_{\rm CP,neat}=0.93$, 1.02, 1.12) and r values indicated in the legend. The anion—cation distance cutoff is 4.5 Å for LiClO₄.

CONCLUSIONS

In this work, we use GEMC simulations to investigate the thermodynamics and structure of OEO/salt solutions and the liquid-liquid equilibria of squalane/OEO blends to provide insights into the irregular phase behavior of salt-doped polymer blends. Through simulations focusing on low-molecular-weight OEO chains of different lengths doped with alkali metal salts (considering ions with different sizes), we provide a comprehensive correlation for the cohesive energy density, Π_{CED} , of OEO/salt mixtures as a function of chain length, temperature, ion type, and concentration. Structural analysis from simulation trajectories reveals interesting molecular-level details. Cation-EO coordination numbers are calculated through various approaches, and using the first minimum in the corresponding cation-EO coordination (instead of a common cutoff distance) together with the integrated cation-EO interaction energy yields a coordination picture consistent with the trends in Π_{CED} . Ion aggregation is found to be very significant even when EO groups outnumber anions by a factor of 100. Despite the large effects of ions on Π_{CED} of the OEO/ salt mixtures and on the enthalpy of vaporization for OEO chains, the vapor pressure of EO pentamers decreases by only 10% in the presence of LiF at $[Li^+]/[EO] \approx 0.010$. Thus, the enthalpic stabilization for solvation in the salt-doped mixture is largely compensated by an increased entropic cost. Accounting for ion aggregation through the van't Hoff factor yields a consistent trend for the relative vapor pressure decrease when changing electrolyte and temperature.

We perform additional simulations and experiments to investigate the effect of LiClO₄ doping on the phase diagram of a squalane/EO-pentamer blend and find a very satisfactory agreement between experiment, simulation, and predictions of the Ren–Nakamura–Wang theory. The unexpected shape of the phase diagram is rationalized by an increase in the ion concentration of the OEO-rich phase at higher temperatures, which significantly reduces the uptake of squalane but, due to enthalpy—entropy compensation, does not significantly alter the escaping tendency of the EO pentamer.

In contrast with the assumptions underlying the Ren-Nakamura-Wang theory, different binding energies between cations and ether oxygens, changes in the cation-EO coordination, and a relatively large population of ion pairing/clustering are found in the structural analysis. We surmise that the cation-induced cross-linking between OEO chains and ion pairing/clustering effects are inherently competitive among the salts covered in this study and thus cannot be decoupled. On the other hand, the coupling of these effects greatly reduces ion-specific effects on the phase behavior (where significant changes in enthalpic and entropic contributions mostly offset each other) and may partially mask differences between fixed-charge force fields and those accounting for induction and charge-transfer effects.

ASSOCIATED CONTENT

Supporting Information

The Supporting Information is available free of charge at https://pubs.acs.org/doi/10.1021/acs.macromol.0c02270.

Simulation details, numerical data, and additional figures (PDF)

AUTHOR INFORMATION

Corresponding Authors

Timothy P. Lodge — Department of Chemical Engineering and Material Science, University of Minnesota, Minneapolis, Minnesota 55455-0132, United States; Department of Chemistry, University of Minnesota, Minneapolis, Minnesota 55455-0431, United States; orcid.org/0000-0001-5916-8834; Email: lodge@umn.edu

J. Ilja Siepmann — Department of Chemical Engineering and Material Science and Chemical Theory Center, University of Minnesota, Minneapolis, Minnesota 55455-0132, United States; Department of Chemistry, University of Minnesota, Minneapolis, Minnesota 55455-0431, United States; orcid.org/0000-0003-2534-4507; Email: siepmann@umn.edu

Authors

Zhengyuan Shen — Department of Chemical Engineering and Material Science and Chemical Theory Center, University of Minnesota, Minneapolis, Minnesota 55455-0132, United States; Department of Chemistry, University of Minnesota, Minneapolis, Minnesota 55455-0431, United States

Qile P. Chen — Department of Chemical Engineering and Material Science and Chemical Theory Center, University of Minnesota, Minneapolis, Minnesota 55455-0132, United States; Department of Chemistry, University of Minnesota, Minneapolis, Minnesota 55455-0431, United States;

orcid.org/0000-0003-2697-8763

Shuyi Xie – Department of Chemistry, University of Minnesota, Minneapolis, Minnesota 55455-0431, United States; orcid.org/0000-0001-7966-1239

Complete contact information is available at: https://pubs.acs.org/10.1021/acs.macromol.0c02270

Notes

The authors declare no competing financial interest.

ACKNOWLEDGMENTS

This work was primarily supported by the National Science Foundation through the University of Minnesota MRSEC

under Award DMR-2011401. Computer resources were provided by this NSF award and by the Minnesota Supercomputing Institute.

REFERENCES

4849.

- (1) Tarascon, J. M.; Armand, M. Issues and Challenges Facing Rechargeable Lithium Batteries. *Nature* **2001**, *414*, 359–367.
- (2) Lodge, T. P. A Unique Platform for Materials Design. *Science* **2008**, 321, 50–51.
- (3) Devaux, D.; Glé, D.; Phan, T. N.; Gigmes, D.; Giroud, E.; Deschamps, M.; Denoyel, R.; Bouchet, R. Optimization of Block Copolymer Electrolytes for Lithium Metal Batteries. *Chem. Mater.* **2015**, 27, 4682–4692.
- (4) Ruzette, A.-V. G.; Soo, P. P.; Sadoway, D. R.; Mayes, A. M. Melt-Formable Block Copolymer Electrolytes for Lithium Rechargeable Batteries. *J. Electrochem. Soc.* **2001**, *148*, A537.
- (5) Epps, T. H.; Bailey, T. S.; Waletzko, R.; Bates, F. S. Phase Behavior and Block Sequence Effects in Lithium Perchlorate-Doped Poly(isoprene-b-styrene-b-ethylene oxide) and Poly (styrene-b-isoprene-b-ethylene oxide) Triblock Copolymers. *Macromolecules* **2003**, *36*, 2873–2881.
- (6) Wang, J.-Y.; Chen, W.; Russell, T. P. Ion-Complexation-Induced Changes in the Interaction Parameter and the Chain Conformation of PS-b-PMMA Copolymers. *Macromolecules* **2008**, *41*, 4904–4907.
- (7) Young, W. S.; Epps, T. H. Salt Doping in PEO-Containing Block Copolymers: Counterion and Concentration Effects. *Macromolecules* **2009**, 42, 2672–2678.
- (8) Wanakule, N. S.; Virgili, J. M.; Teran, A. A.; Wang, Z. G.; Balsara, N. P. Thermodynamic Properties of Block Copolymer Electrolytes Containing Imidazolium and Lithium Salts. *Macromolecules* **2010**. *43*, 8282–8289.
- (9) Naidu, S.; Ahn, H.; Gong, J.; Kim, B.; Ryu, D. Y. Phase Behavior and Ionic Conductivity of Lithium Perchlorate-Doped Polystyrene-b-Poly(2-inylpyridine) Copolymer. *Macromolecules* **2011**, *44*, 6085–6093.
- (10) Gunkel, I.; Thurn-Albrecht, T. Thermodynamic and Structural Changes in Ion-Containing Symmetric Diblock Copolymers: A Small-Angle X-ray Scattering Study. *Macromolecules* **2012**, *45*, 283–291.
- (11) Teran, A. A.; Balsara, N. P. Thermodynamics of Block Copolymers with and without Salt. *J. Phys. Chem. B* **2014**, *118*, 4–17. (12) Irwin, M. T.; Hickey, R. J.; Xie, S.; Bates, F. S.; Lodge, T. P. Lithium Salt-Induced Microstructure and Ordering in Diblock Copolymer/Homopolymer Blends. *Macromolecules* **2016**, *49*, 4839–
- (13) Wang, Z.-G. Effects of Ion Solvation on the Miscibility of Binary Polymer Blends. *J Phys. Chem. B* **2008**, *112*, 16205–16213.
- (14) Nakamura, I.; Wang, Z. G. Salt-Doped Block Copolymers: Ion Distribution, Domain Spacing and Effective χ Parameter. *Soft Matter* **2012**, *8*, 9356–9367.
- (15) Sing, C. E.; Zwanikken, J. W.; Olvera De La Cruz, M. Ion Correlation-Induced Phase Separation in Polyelectrolyte Blends. *ACS Macro Lett.* **2013**, *2*, 1042–1046.
- (16) Sing, C. E.; Olvera De La Cruz, M. Polyelectrolyte Blends and Nontrivial Behavior in Effective Flory-Huggins Parameters. *ACS Macro Lett.* **2014**, *3*, 698–702.
- (17) Sing, C. E.; Zwanikken, J. W.; Olvera De La Cruz, M. Theory of Melt Polyelectrolyte Blends and Block Copolymers: Phase Behavior, Surface Tension, and Microphase Periodicity. *J. Chem. Phys.* **2015**, 142, No. 034902.
- (18) Kwon, H. K.; Zwanikken, J. W.; Shull, K. R.; Olvera De La Cruz, M. Theoretical Analysis of Multiple Phase Coexistence in Polyelectrolyte Blends. *Macromolecules* **2015**, *48*, 6008–6015.
- (19) Ren, C. L.; Nakamura, I.; Wang, Z. G. Effects of Ion-Induced Cross-Linking on the Phase Behavior in Salt-Doped Polymer Blends. *Macromolecules* **2016**, *49*, 425–431.
- (20) Hou, K. J.; Qin, J. Solvation and Entropic Regimes in Ion-Containing Block Copolymers. *Macromolecules* **2018**, *51*, 7463–7475.

- (21) Qin, J.; De Pablo, J. J. Ordering Transition in Salt-Doped Diblock Copolymers. *Macromolecules* **2016**, *49*, 3630–3638.
- (22) Chu, W.; Qin, J.; De Pablo, J. J. Ion Distribution in Microphase-Separated Copolymers with Periodic Dielectric Permittivity. *Macromolecules* **2018**, *51*, 1986–1991.
- (23) Hou, K. J.; Loo, W. S.; Balsara, N. B.; Qin, J. Comparing Experimental Phase Behavior of Ion-Doped BlockCopolymers with Theoretical Predictions Based on Selective IonSolvation. *Macromolecules* **2020**, *53*, 3956–3966.
- (24) Kim, S. H.; Misner, M. J.; Yang, L.; Gang, O.; Ocko, B. M.; Russell, T. P. Salt Complexation in Block Copolymer Thin Films. *Macromolecules* **2006**, *39*, 8473–8479.
- (25) Kumar, R.; Muthukumar, M. Microphase Separation in Polyelectrolytic Diblock Copolymer Melt: Weak Segregation Limit. *J. Chem. Phys* **2007**, *126*, No. 214902.
- (26) Wang, J. Y.; Chen, W.; Roy, C.; Sievert, J. D.; Russell, T. P. Influence of Ionic Complexes on Phase Behavior of Polystyrene-b-Poly(methyl methacrylate) Copolymers. *Macromolecules* **2008**, *41*, 963–969.
- (27) Wanakule, N. S.; Panday, A.; Mullin, S. A.; Gann, E.; Hexemer, A.; Balsara, N. P. Ionic Conductivity of Block Copolymer Electrolytes in the Vicinity of Order-Disorder and Order-Order Transitions. *Macromolecules* **2009**, 42, 5642–5651.
- (28) Brown, J. R.; Seo, Y.; Hall, L. M. Ion Correlation Effects in Salt-Doped Block Copolymers. *Phys. Rev. Lett.* **2018**, *120*, No. 127801.
- (29) Xie, S.; Lodge, T. P. Phase Behavior of Binary Polymer Blends Doped with Salt. *Macromolecules* **2018**, *51*, 266–274.
- (30) Hildebrand, J. H.; Scott, R. L. The Solubility of Nonelectrolytes; Dover: New York, 1964.
- (31) Huggins, M. L. Solutions of Long Chain Compounds. J. Chem. Phys. 1941, 9, 440.
- (32) Flory, P. J. Thermodynamics of High Polymer Solutions. J. Chem. Phys. 1941, 9, 660–661.
- (33) Flory, P. J. Thermodynamics of High Polymer Solutions. J. Chem. Phys. 1942, 10, 51–61.
- (34) Borodin, O.; Smith, G. D. Molecular Dynamics Simulations of Poly(ethylene oxide)/Lil Melts. 1. Structural and Conformational Properties. *Macromolecules* **1998**, *31*, 8396–8406.
- (35) Borodin, O.; Smith, G. D. Mechanism of Ion Transport in Amorphous Poly(ethylene oxide)/LiTFSI from Molecular Dynamics Simulations. *Macromolecules* **2006**, *39*, 1620–1629.
- (36) Siqueira, L. J. A.; Ribeiro, M. C. C. Molecular Dynamics Simulation of the Polymer Electrolyte Poly(ethyleneoxide)/LiClO₄. I. Structural Properties. *J. Chem. Phys.* **2005**, *122*, No. 194911.
- (37) Siqueira, L. J. A.; Ribeiro, M. C. C. Molecular Dynamics Simulation of the Polymer Electrolyte Poly (ethylene oxide)/LiClO₄. II. Dynamical Properties. *J. Chem. Phys.* **2006**, *125*, No. 214903.
- (38) Lin, K. J.; Maranas, J. K. Cation Coordination and Motion in a Poly(ethylene oxide)-Based Single Ion Conductor. *Macromolecules* **2012**, *45*, 6230–6240.
- (39) Molinari, N.; Mailoa, J. P.; Kozinsky, B. Effect of Salt Concentration on Ion Clustering and Transport in Polymer Solid Electrolytes: A Molecular Dynamics Study of PEO-LiTFSI. *Chem. Mater.* **2018**, *30*, 6298–6306.
- (40) Panagiotopoulos, A. Z. Direct Determination of Phase Coexistence Properties of Fluids by Monte Carlo Simulation in a New Ensemble. *Mol. Phys.* **1987**, *61*, 813–826.
- (41) Panagiotopoulos, A. Z.; Quirke, N.; Stapleton, M.; Tildesley, D. J. Phase Equilibria by Simulation in the Gibbs Ensemble Alternative Derivation, Generalization and Application to Mixture and Membrane Equilibria. *Mol. Phys.* **1988**, *63*, 527–545.
- (42) Siepmann, J. I.; Martin, M. G.; Chen, B.; Wick, C. D.; Stubbs, J. M.; Potoff, J. J.; Eggimann, B. L.; McGrath, M. J.; Zhao, X. S.; Anderson, K. E. et al. *Monte Carlo for Complex Chemical Systems—Minnesota*, version 17.1; University of Minnesota: Minneapolis, MN, 2017.
- (43) Cortés Morales, A. D.; Econonmou, I. G.; Peters, C. J.; Siepmann. Influence of simulation protocols on the efficiency of Gibbs ensemble Monte Carlo simulations. *Mol. Simul.* **2013**, *39*, 1135–1142.

- (44) Chen, Q. P.; Xie, S.; Foudazi, R.; Lodge, T. P.; Siepmann, J. I. Understanding the Molecular Weight Dependence of and the Effect of Dispersity on Polymer Blend Phase Diagrams. *Macromolecules* **2018**, *51*, 3774–3787.
- (45) Stubbs, J. M.; Potoff, J. J.; Siepmann, J. I. Transferable Potentials for Phase Equilibria. 6. United-Atom Description for Ethers, Glycols, Ketones, and Aldehydes. *J. Phys. Chem. B* **2004**, *108*, 17596–17605.
- (46) Jensen, K. P.; Jorgensen, W. L. Halide, Ammonium, and Alkali Metal Ion Parameters for Modeling Aqueous Solutions. *J. Chem. Theory Comput.* **2006**, *2*, 1499–1509.
- (47) Cadena, C.; Maginn, E. J. Molecular Simulation Study of Some Thermophysical and Transport Properties of Triazolium-Based Ionic Liquids. *J. Phys. Chem. B* **2006**, *110*, 18026–18039.
- (48) Wood, W. W.; Parker, F. R. Monte Carlo Equation of State of Molecules Interacting with the Lennard-Jones Potential. I. A Supercritical Isotherm at about Twice the Critical Temperature. *J. Chem. Phys.* **1957**, 27, 720–733.
- (49) Allen, M. P.; Tildesley, D. J. Computer Simulation of Liquids; Clarendon Press: Oxford, 1987.
- (50) Vlugt, T. J. H.; Martin, M. G.; Smit, B.; Siepmann, J. I.; Krishna, R. Improving the Efficiencyof the Configurational-bias Monte Carlo Algorithm. *Mol. Phys.* **1998**, *94*, 727–733.
- (51) Martin, M. G.; Siepmann, J. I. Novel Configurational-Bias Monte Carlo Method for Branched Molecules. Transferable Potentials for Phase Equilibria. 2. United-Atom Description of Branched Alkanes. J. Phys. Chem. B 1999, 103, 4508–4517.
- (52) De Pablo, J. J.; Prausnitz, J. M. Phase Equilibria for Fluid Mixtures from Monte-Carlo Simulation. *Fluid Phase Equilib.* **1989**, *53*, 177–189.
- (53) Martin, M. G.; Siepmann, J. I. Predicting Multicomponent Phase Equilibria and Free Energies of Transfer for Alkanes by Molecular Simulation. *J. Am. Chem. Soc.* **1997**, *119*, 8921–8924.
- (54) Chen, B.; Siepmann, J. I. Microscopic Structure and Solvation in Dry and Wet Octanol. *J. Phys. Chem. B* **2006**, *110*, 3555–3563.
- (55) Chen, Q. P.; Chu, J. D.; Dejaco, R. F.; Lodge, T. P.; Siepmann, J. I. Molecular Simulation of Olefin Oligomer Blend Phase Behavior. *Macromolecules* **2016**, *49*, 3975–3985.
- (56) Bicerano, J. Prediction of Polymer Properties, 2nd ed.; Marcel Dekker: New York, NY, 1996; pp 108-136.
- (57) Krishnamoorti, R.; Graessley, W. W.; Dee, G. T.; Walsh, D. J.; Fetters, L. J.; Lohse, D. J. Pure Component Properties and Mixing Behavior in Polyolefin Blends. *Macromolecules* **1996**, *29*, 367–376.
- (58) Maranas, J. K.; Mondello, M.; Grest, G. S.; Kumar, S. K.; Debenedetti, P. G.; Graessley, W. W. Liquid Structure, Thermodynamics, and Mixing Behavior of Saturated Hydrocarbon Polymers. 1. Cohesive Energy Density and Internal Pressure. *Macromolecules* 1998, 31, 6991–6997
- (59) Rai, N.; Siepmann, J. I.; Schultz, N. E.; Ross, R. B. Pressure Dependence of the Hildebrand Solubility Parameter and the Internal Pressure: Monte Carlo Simulations for External Pressures up to 300 MPa. J. Phys. Chem. C 2007, 111, 15634–15641.
- (60) White, R. P.; Lipson, J. E. G. Free Volume, Cohesive Energy Density, and Internal Pressure as Predictors of Polymer Miscibility. *Macromolecules* **2014**, *47*, 3959–3968.
- (61) Maranas, J. K.; Mondello, M.; Grest, G. S.; Kumar, S. K.; Debenedetti, P. G.; Graessley, W. W. Liquid structure, Thermodynamics, and Mixing Behavior of Saturated Hydrocarbon Polymers. 1. Cohesive Energy Density and Internal Pressure. *Macromolecules* 1998, 31, 6991–6997.
- (62) Marcus, Y. Structure of Mixtures of Water and Methanol Derived from TheirCohesive Energy Densities and Internal Pressures from SubambientTemperatures to 473 K. J. Phys. Chem. B 2017, 121, 863–866.
- (63) Morrow, T. I.; Maginn, E. J. Molecular Dynamics Study of the Ionic Liquid 1-n-Butyl-3-methylimidazoliumHexafluorophosphate. *J. Phys. Chem. B* **2002**, *106*, 12807–12813.

- (64) Fullerton-Shirey, S. K.; Maranas, J. K. Structure and Mobility of PEO/LiClO₄ Solid Polymer Electrolytes Filled with Al₂O₃ Nanoparticles. *J. Phys. Chem. C* **2010**, *114*, 9196–9206.
- (65) Tanaka, N. Prediction of Solubility Parameter from Thermal Transition Behaviour in Polymers. *Polymer* **1992**, *33*, 623–626.
- (66) Chen, X.; Yuan, C.; Wong, C. K. Y.; Zhang, G. Molecular Modeling of Temperature Dependence of Solubility Parameters for Amorphous Polymers. *J. Mol. Model.* **2012**, *18*, 2333–2341.
- (67) Graessley, W. W.; Krishnamoorti, R.; Reichart, G. C.; Balsara, N. P.; Fetters, L. J.; Lohse, D. J. Regular and Irregular Mixing Behavior in Blends of SaturatedHydrocarbon Polymers. *Macromolecules* 1995, 28, 1260–1270.
- (68) Fox, T. G., Jr.; Flory, P. J. Second-Order Transition Temperatures and Related Properties of Polystyrene. I. Influence of Molecular Weight. *J. Appl. Phys.* **1950**, *21*, 581.
- (69) Dee, G. T.; Ougizawa, T.; Walsh, D. J. The Pressure-Volume-Temperature Properties of Polyethylene, Poly (dimethyl siloxane), Poly (ethylene glycol) and Poly (propylene glycol) as a Function of Molecular Weight. *Polymer* **1992**, 33, 3462–3469.
- (70) Dee, G. T.; Sauer, B. B. The Cohesive Energy Density of Polymers and its Relationship to Surface Tension, Bulk Thermodynamic Properties, and Chain Structure. *J. Appl. Polym. Sci.* **2017**, *134*, No. 44431.
- (71) Maitland, G. C.; Rigby, M.; Smith, E. B.; Wakeham, A. *Intermolecular Forces: Their Origin and Determination*; Pergamon Press: Oxford, U.K., 1987.
- (72) Gong, H. P.; Hocky, G.; Freed, K. F. Influence of nonlinear electrostatics on transfer energies between liquid phases: Charge burial is far less expensive than Born model. *Proc. Natl. Acad. Sci. U.S.A.* **2008**, *105*, 11146–11151.
- (73) Nakamura, I. Effects of Dielectric Inhomogeneity and Electrostatic Correlation on the Solvation Energy of Ions in Liquids. *J. Phys. Chem. B* **2018**, 122, 6064–6071.
- (74) Shock, C. J.; Stevens, M. J.; Frischknecht, A. L.; Nakamura, I. Solvation Energy of Ions in a Stockmayer Fluid. *J. Phys. Chem. B* **2020**, 124, 4598–4604.
- (75) Timachova, K.; Watanabe, H.; Balsara, N. P. Effect of Molecular Weight and Salt Concentration on Ion Transport and the Transference Number in Polymer Electrolytes. *Macromolecules* **2015**, *48*, 7882–7888.
- (76) Webb, M. A.; Jung, Y.; Pesko, D. M.; Savoie, B. M.; Yamamoto, U.; Coates, G. W.; Balsara, N. P.; Wang, Z.-G.; Miller, T. F., III Systematic Computational and Experimental Investigation of Lithium-Ion Transport Mechanisms in Polyester-Based Polymer Electrolytes. *ACS Cent. Sci.* 2015, *1*, 198–205.
- (77) Neyertz, S.; Brown, D. Local Structure and Mobility of Ions in Polymer Electrolytes: A Molecular Dynamics Simulation Study of the Amorphous PEO_xNaI System. *J. Chem. Phys.* **1996**, *104*, *3797*.
- (78) Ray, D.; Feller, D.; More, M. B.; Glendening, E. D.; Armentrout, P. B. Cation-Ether Complexes in the Gas Phase: Bond Dissociation Energies and Equilibrium Structures of Li⁺(1,2-dimethoxyethane)_{xy} x = 1 and 2, and Li⁺(12-crown-4). *J. Phys. Chem. A.* **1996**, 100, 16116–16125.
- (79) More, M. B.; Ray, D.; Armentrout, P. B. Cation-Ether Complexes in the Gas Phase: Bond Dissociation Energies of $M^+(dimethyl \ ether)_x$, x = 1-3; $M^+(1,2-dimethoxyethane)_x$, x = 1 and 2; and $M^+(12-crown-4)$, where M = Rb and Cs. *J. Phys. Chem. A* **1997**, 101, 7007–7017.
- (80) Memboeuf, A.; Vékey, K.; Lendvay, G. Structure and Energetics of Poly(ethylene glycol) Cationized by Li⁺, Na⁺, K⁺ and Cs⁺: a First-Principles Study. *Eur. J. Mass Spectrom.* **2011**, *17*, 33.
- (81) Sinha, K.; Maranas, J. K. Does Ion Aggregation Impact Polymer Dynamics and Conductivity in PEO-Based Single ion Conductors. *Macromolecules* **2014**, 47, 2718–2726.
- (82) Lin, K. J.; Maranas, J. K. Does Decreasing Ion-Ion Association Improve Cation Mobility in Single Ion Conductors. *Phys. Chem. Chem. Phys.* **2013**, *15*, 16143–16151.

- (83) Lin, K.-J.; Li, K.; Maranas, J. K. Differences Between Polymer/Salt and Single Ion Conductor Solid Polymer Electrolytes. *RSC Adv.* **2013**, *3*, 1564–1571.
- (84) Lin, K. J.; Maranas, J. K. Superionic Behavior in Polyethylene-Oxide-Based Single-Ion Conductors. *Phys. Rev. E* **2013**, *88*, No. 052602.
- (85) Salomon, M.; Xu, M.; Eyring, E. M.; Petrucci, S. Molecular Structure and Dynamics of LiClO₄-Polyethylene Oxide-400 (Dimethyl Ether and Diglycol Systems) at 25 °C. *J. Phys. Chem. B.* **1994**, 98, 8234–8244.
- (86) Ducasse, L.; Dussauze, M.; Grondin, J.; Lassègues, J. C.; Naudin, C.; Servant, L. Spectroscopic Study of Poly(ethylene oxide)₆: LiX Complexes (X = PF₆, AsF₆, SbF₆, ClO₄. *Phys. Chem. Chem. Phys.* **2003**, *5*, 567–574.
- (87) Brodin, A.; Mattson, B.; et al. Ionic Configurations in PEO Based Electrolytes Endcapped by CH₃-, OH- and SO₃- Groups. *Solid State Ionics* **1996**, 85, 111–120.
- (88) Reiche, A.; Tübke, J.; Siury, K.; Sandner, B.; Fleischer, G.; Wartewig, S.; Shashkov, S. Gel Electrolytes with Plasticizers of Different Polarity. *Solid State Ionics* **1996**, 85, 121–127.
- (89) Wiencierz, M.; Stolwijk, N. A. Systematics of Ionic Transport and Pair Formation in Amorphous PEO-NaI Polymer Electrolytes. *Solid State Ionics* **2012**, 212, 88–99.
- (90) Stolwijk, N. A.; Wiencierz, M.; Heddier, C.; Kösters, J. What can we learn from ionic conductivity measurements in polymer electrolytes? A case study on Poly(ethylene oxide) (PEO)-NaI and PEO-LiTFSI. *J. Phys. Chem. B* **2012**, *116*, 3065–3074.
- (91) Edman, L. Ion Assiciation and Ion Solvation Effects at the Crystalline-Amorphous Phase Transition in PEO-LiTFSI. *J. Phys. Chem. B* **2000**, *104*, 7254–7258.
- (92) Mao, G.; Saboungi, M. L.; Price, D. L.; Badyal, Y. S.; Fischer, H. E. Lithium Environment in PEO-LiClO₄ Polymer Electrolyte. *Europhys. Lett.* **2001**, *54*, 347–353.
- (93) Ben-Naim, A. Statistical Thermodynamics for Chemists and Biochemists; Plenum: New York, 1992.
- (94) Ben-Naim, A.; Mazo, R. Size Dependence of Solvation Gibbs Energies: A Critique and a Rebuttal of Some Recent Publications. *J. Phys. Chem. B* **1997**, *101*, 11221–11225.
- (95) Martin, M. G.; Siepmann, J. I. Calculating Gibbs Free Energies of Transfer from Gibbs Ensemble Monte Carlo Simulations. *Theor. Chem. Acc.* **1998**, 99, 347–350.
- (96) Widom, B. Some Topics in the Theory of Fluids. *J. Chem. Phys.* **1963**, 39, 2808–2812.
- (97) Jenkins, H. D. B.; Thakur, K. P. Reappraisal of Thermochemical Radii for Complex Ions. *J. Chem. Educ.* **1979**, *56*, No. 576.
- (98) Ue, M. Mobility and Ionic Association of Lithium and Quaternary Ammonium Salts in Propylene Carbonate and γ -Butyrolactone. *J. Electrochem. Soc.* **1994**, *141*, 3336–3342.